



Photoluminescence Properties of Two Closely Related Isostructural Series Based on Anderson-Evans Cluster Coordinated With Lanthanides

$[\text{Ln}(\text{H}_2\text{O})_7\{\text{X}(\text{OH})_6\text{Mo}_6\text{O}_{18}\}] \cdot y\text{H}_2\text{O}$, $\text{X} = \text{Al}, \text{Cr}$

Shailabh Tewari¹, Mohammad Adnan², Balendra¹, Vineet Kumar¹, Gaurav Jangra¹, Gaddam Vijaya Prakash^{2*} and Arunachalam Ramanan^{1*}

OPEN ACCESS

Edited by:

Tatjana N. Parac-Vogt,
KU Leuven, Belgium

Reviewed by:

Aleksandar Kondinski,
KU Leuven, Belgium
Svetlana V. Eliseeva,
UPR4301 Centre de Biophysique
Moléculaire (CBM), France

*Correspondence:

Gaddam Vijaya Prakash
prakash@physics.iitd.ac.in
Arunachalam Ramanan
aramanan@chemistry.iitd.ac.in

Specialty section:

This article was submitted to
Inorganic Chemistry,
a section of the journal
Frontiers in Chemistry

Received: 08 June 2018

Accepted: 05 December 2018

Published: 07 January 2019

Citation:

Tewari S, Adnan M, Balendra, Kumar
V, Jangra G, Prakash GV and
Ramanan A (2019)
Photoluminescence Properties of Two
Closely Related Isostructural Series
Based on Anderson-Evans Cluster
Coordinated With Lanthanides
 $[\text{Ln}(\text{H}_2\text{O})_7\{\text{X}(\text{OH})_6\text{Mo}_6\text{O}_{18}\}] \cdot y\text{H}_2\text{O}$,
 $\text{X} = \text{Al}, \text{Cr}$. *Front. Chem.* 6:631.
doi: 10.3389/fchem.2018.00631

¹ Department of Chemistry, Indian Institute of Technology Delhi, New Delhi, India, ² Department of Physics, Indian Institute of Technology Delhi, New Delhi, India

The paper describes synthesis and structural characterization of the whole series of two closely related lanthanide coordinated chromium or aluminum hexamolybdates (Anderson-Evans cluster) including twelve new members hitherto unreported: $[\text{Ln}(\text{H}_2\text{O})_7\{\text{X}(\text{OH})_6\text{Mo}_6\text{O}_{18}\}] \cdot 4\text{H}_2\text{O}$ and $[\text{Ln}(\text{H}_2\text{O})_7\{\text{X}(\text{OH})_6\text{Mo}_6\text{O}_{18}\} \text{Ln}(\text{H}_2\text{O})_7\{\text{X}(\text{OH})_6\text{Mo}_6\text{O}_{18}\}] \cdot 16\text{H}_2\text{O}$ where $\text{X} = \text{Al}$ or Cr and $\text{Ln} = \text{La}, \text{Ce}, \text{Pr}, \text{Nd}, \text{Sm}, \text{Eu}, \text{Gd}, \text{Tb}, \text{Dy}, \text{Ho}, \text{Er}, \text{Tm}, \text{Yb}, \text{Lu},$ and Y . Crystal structures of all the solids were established by powder and single crystal X-ray diffraction techniques. The two series are dictated by a different aggregation of the same set of molecular species: Lighter lanthanides favor coordination interaction between lanthanide ions and molybdate cluster forming 1D chains (Series I) while the heavier lanthanides result in the stacking of a cation, a pair of lanthanide hydrates coordinating to the cluster, and an anion, the discrete cluster is further stabilized through a large number of water molecules (Series II). Crystallization with Er^{3+} and Tm^{3+} ions results in a concomitant mixture of Series I and II. Photoluminescence of single crystals of all the chromium molybdates was dominated by a ruby-like emission including those which contain optically active ions Pr, Sm, Eu, Tb, Dy, and Tm. In contrast, aluminum analogs showed photoluminescence corresponding to characteristic lanthanide emissions. Our results strongly suggest a possible energy transfer from f levels of lanthanide ions to d levels of chromium (III) causing the quenching of lanthanide emission when coordinated with chromium molybdates. Intensity measurements showed that the emission from chromium molybdates are almost two orders of magnitude lower than naturally occurring ruby with broader line widths at room temperature.

Keywords: Anderson-Evans cluster, structural chemistry, lanthanides, chromium molybdate, aluminum molybdate, photoluminescence

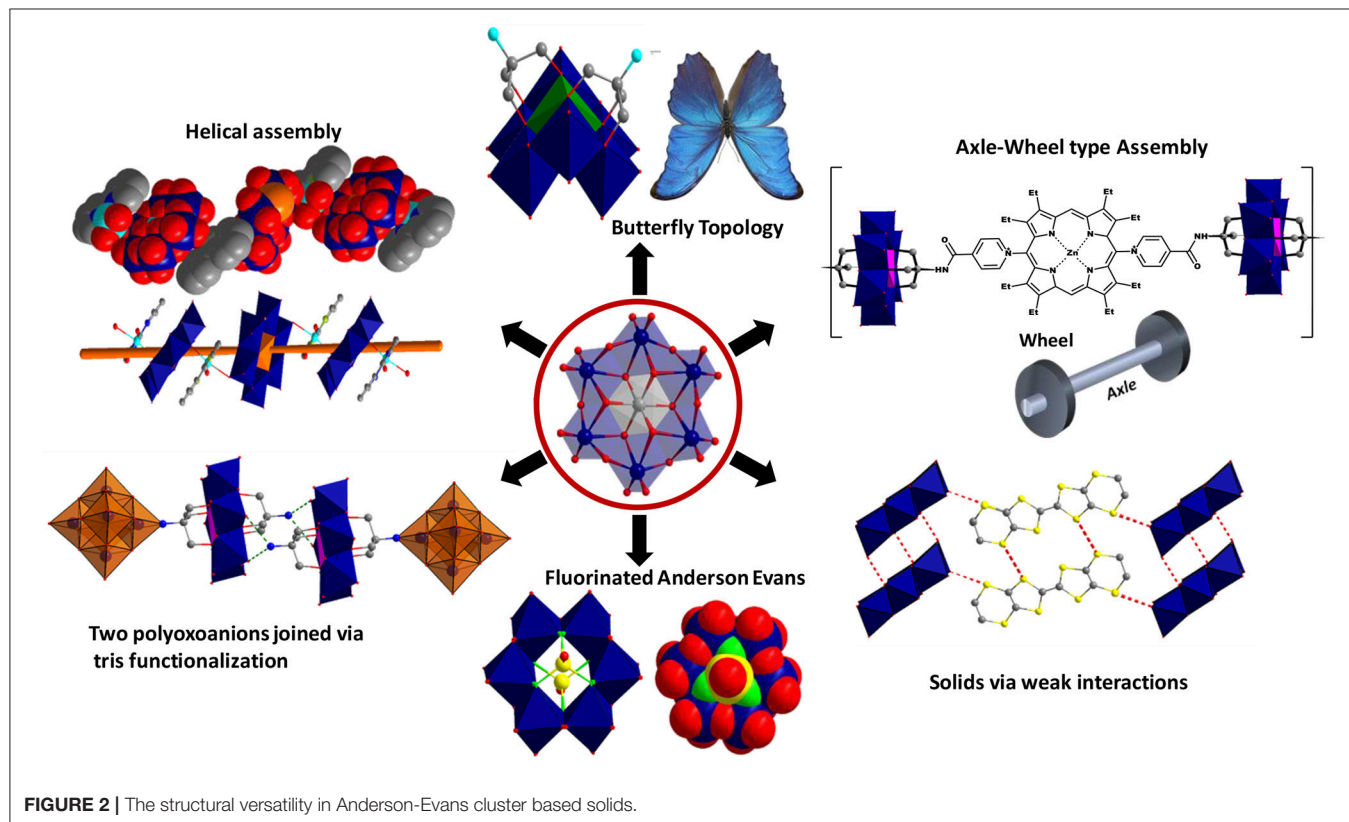
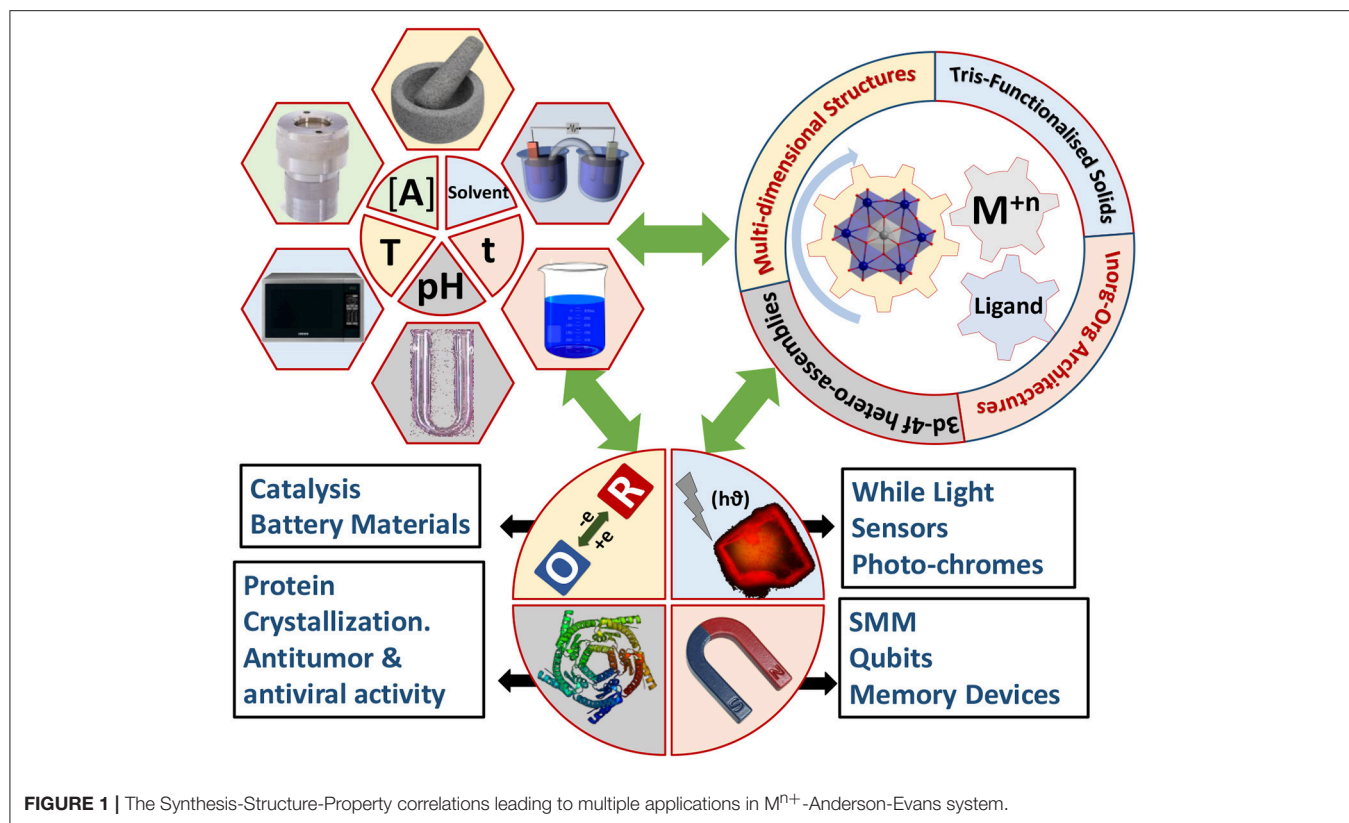
INTRODUCTION

Polyoxomolybdates (POM), an important branch in polyoxometalate chemistry, presents an unrivaled structural chemistry and physicochemical properties providing immense opportunities as well as considerable challenges in creating new functional materials (Hill, 1998; Pope, 2002; Li and Xu, 2011; Eldik and Cronin, 2017; Song, 2018). Among the POM anions, a hetero polyoxomolybdate of the composition, $[X^{n+}Mo_6O_{24}H_y]^{(12-n-y)-}$, was found to be a dominant building block in several solids (Blazevic and Rompel, 2016). Its molecular structure, first proposed almost eighty years ago (Anderson, 1937), was established experimentally by refining the X-ray crystallographic data obtained for the tellurium salts, $(NH_4)_6\{TeMo_6O_{24}\cdot 7H_2O$ and $K_6\{TeMo_6O_{24}\cdot 7H_2O$ (Evans, 1948). Anderson-Evans cluster, as it has been known since, is made of six edge-shared distorted $\{MoO_6\}$ octahedra and the central cavity thus formed is occupied by slightly flattened, $X(OH)_6$, heteroatom octahedron. The cluster assumes a near D_{3d} symmetry with dimensions $\sim 8.6 \times 8.6 \times 2.7$ Å and has been isolated with fifteen different heteroatoms till now [X: **Al** (Lee et al., 1991; Manikumari et al., 2002; Shivaiah et al., 2002; Martin et al., 2004; Shivaiah and Das, 2005; Liu et al., 2006; Dhara et al., 2007; Cao et al., 2008; Zhou et al., 2009), **Cr** (Perloff, 1970; An et al., 2006; Yu et al., 2006; Lee, 2007; Zhou and Yang, 2007; Shi D. et al., 2008; Shi D. M. et al., 2008; Zhang et al., 2008, 2014; Singh et al., 2010b, 2014; Li et al., 2011; Singh and Ramanan, 2011; Kumar et al., 2014a; Joo et al., 2015), **Mn** (He et al., 2012; Oms et al., 2012; Rosnes et al., 2012, 2013; Yan et al., 2012; Zhang et al., 2012, 2015a,b; Hutin et al., 2013; Ai et al., 2014; Yvon et al., 2014), **Fe** (Wu et al., 2001), **Co** (Nolan et al., 1996; Panneerselvam et al., 1996; Lee and Joo, 2000a; Lee et al., 2001; Martin et al., 2004), **Ni** (Lee et al., 2002; Liu et al., 2007; Liu F.-X. et al., 2008), **Cu** (Ito et al., 1989), **Zn** (Allen et al., 1997), **Ga** (Mensingher et al., 2008; Himeno et al., 2009), **Te** (Evans, 1948; Kondo et al., 1980; Robl and Frost, 1993a,b; Lorenzo-Luis et al., 1999; Drewes et al., 2004a,b; Charushnikova et al., 2005; Drewes and Krebs, 2005; Gao et al., 2007; Liu Y. et al., 2008; Yan et al., 2008), **Rh** (Ozawa et al., 1991), **Pd** (Ozawa et al., 1991), **Sb** (Ogawa et al., 1988; Yan et al., 2014), **I** (Kondo et al., 1980; Rosu and Weakley, 2000; An et al., 2005) and **Pt** (Lee and Sasaki, 1984; Lee, 1994; Lee and Joo, 2000b, 2004, 2006a,b, 2007)]. The “disc-shaped” geometry and the nucleophilicity of the twelve terminal oxygens (O_t) render the POM cluster as an attractive ligand to engineer helices (Shivaiah et al., 2003), stacks or multidimensional frameworks (An et al., 2005; Ritchie and Bryant, 2015) through hydrogen bonding as well as metal-oxygen coordination. Furthermore, the structural versatility of this cluster is unique and can be tuned at the molecular level. It can be modified through the substitution of the triply bridged OH groups with fluoride ions (Michailovski et al., 2009), “axle-wheel” type (Schaming et al., 2010; Allain et al., 2013) with appropriate ligands or bent “butterfly” topologies (Zhang et al., 2017) via suitable functionalization (Figure 2). For this reason, a range of applications, from the much studied luminescent (Ohashi et al., 1982; Yamase and Sugeta, 1993; Ito et al., 2006; Kumar et al., 2014a), catalytic (Tanaka et al., 2012; Bayraq et al.,

2013), anti-tumor (Yamase, 1993; Raza et al., 2012; Shah et al., 2014), anti-viral (Inouye et al., 1993), photochromic (Coué et al., 2007; Song et al., 2008; Pardo et al., 2011; Oms et al., 2012; Allain et al., 2013; Hakouk et al., 2014) and magnetic (Leuenberger and Loss, 2001; Lehmann et al., 2007; Kushch et al., 2009; Wu et al., 2009; Feng et al., 2012) to the recently realized macromolecular crystallography (Bijelic et al., 2014; Mauracher et al., 2014a,b; Bijelic and Rompel, 2015) and functional bio-nanomaterials (Massia and Hubbell, 1991; Aota et al., 1994; Song et al., 2009) are envisaged for solids based on it (Figure 1). Synthesis-structure-function correlation is key to recognize the utility of these solids as futuristic materials.

There has been a renewed interest in the synthesis of lanthanide-based coordination solids with multidimensional structures; the trend is to tune the size, shape and dimensionality between nano to micro level to optimize luminescent properties for a desirable purpose (Binnemans, 2009; Armelao et al., 2010; Bünzli and Eliseeva, 2013; de Bettencourt-Dias, 2014). In this context, a few groups have investigated photoluminescence (PL) of lanthanide-Anderson-Evans cluster based solids (Yusov et al., 2002; Cao et al., 2008; Shi D. M. et al., 2008; Yang et al., 2013; Kumar et al., 2014a). The solid $[Eu(H_2O)_7\{Cr(OH)_6Mo_6O_{18}\} \cdot 4H_2O$ belonging to Series I showed only characteristic emission due to Eu^{3+} ions (Shi D. M. et al., 2008). The solid $[(C_6H_5NO_2)_2Dy(H_2O)_6\{Cr(OH)_6Mo_6O_{18}\} \cdot 2C_6H_5NO_2 \cdot 6H_2O$ showed characteristic emission due to Dy^{3+} ion (Yang et al., 2013). Dinesh et al. observed that Sm^{3+} and Tb^{3+} members of Series I showed only a red emission (Kumar et al., 2014a) reminiscent of ruby, while the lanthanide ion remained optically silent. Another molecular solid containing no lanthanide ions, $[(Hbipy)_2\{Cr(OH)_6Mo_6O_{17}(OH)\}(bipy)]$ also showed a ruby-like emission (Li et al., 2016). It should be mentioned that Yamase and his group were the first to observe the red emission reminiscent of ruby (Yamase and Sugeta, 1993; Ito et al., 2006) in $Na_3[Cr(OH)_6Mo_6O_{18}] \cdot 8H_2O$ at 4.2 K. It was noted that majority of the chromium hexamolybdate based crystals reported in literature, including the aforementioned solids, appeared pink in color. This suggested the domination of red emission arising from chromium ion. The contradicting photoluminescent behavior raised an obvious question, whether the presence or absence of a coordination linkage between the chromium molybdate cluster and lanthanide ions has any influence on their optical properties. This prompted us to explore the structural landscape of the system $Ln^{3+(aq)}\{-X(OH)_6Mo_6O_{18}\} \cdot H_2O$ ($X = Cr^{3+}$ or Al^{3+}).

A structural analysis of the reported solids with the general composition $[Ln(H_2O)_7\{X(OH)_6Mo_6O_{18}\} \cdot yH_2O$, in particular, showed the occurrence of two types: (i) Formation of 1D chains between hydrated $\{Ln(H_2O)_n\}$ and the cluster through extended $-Ln-(O_t\text{-cluster-}O_t)\text{-Ln-}$ leading to **Series I** (Figure S1) of the composition $[Ln(H_2O)_7\{X(OH)_6Mo_6O_{18}\} \cdot 4H_2O$ and (ii) occurrence of a molecular solid (0D) resulting from an aggregation between two discrete units, cationic $[Ln(H_2O)_7\{X(OH)_6Mo_6O_{18}\}Ln(H_2O)_7]^{3+}$ and anionic $\{X(OH)_6Mo_6O_{18}\}^{3-}$ crystallizing into **Series II** (Figure S2)



of the formula $[\text{Ln}(\text{H}_2\text{O})_7\text{Ln}\{\text{X}(\text{OH})_6\text{Mo}_6\text{O}_{18}\}\text{Ln}(\text{H}_2\text{O})_7]\{\text{X}(\text{OH})_6\text{Mo}_6\text{O}_{18}\}\cdot 16\text{H}_2\text{O}$. The lack of systematic synthetic protocol in literature underlined the need to adopt a uniform procedure to crystallize the complete series of solids $[\text{Ln}(\text{H}_2\text{O})_7\{\text{Cr}(\text{OH})_6\text{Mo}_6\text{O}_{18}\}]\cdot x\text{H}_2\text{O}$ with an objective to understand the crystal structures, the origin of its photophysical properties and establish a structure-property correlation. For comparison, we also synthesized the same series with optically inactive aluminum as heteroatom, though a few members have already been reported. Our study has established the growth of the two structurally related members, Series I and II, with similar composition (except for the number of lattice water) as we go along the period. The decrease in size of the lanthanides favors a coordination change from nine to eight and is thus responsible for triggering a slightly different supramolecular assembly. The paper reports the synthesis, structure and photoluminescence properties of the whole series including twelve new members, to the best of our knowledge, hitherto unreported: $[\text{Ln}(\text{H}_2\text{O})_7\{\text{X}(\text{OH})_6\text{Mo}_6\text{O}_{18}\}]\cdot 4\text{H}_2\text{O}$, $\text{X} = \text{Al}$ and $\text{Ln} = \text{Pr, Nd, Tb, Dy}$ and Ho ; $\text{X} = \text{Cr}$ and $\text{Ln} = \text{Tb, Dy}$ and Ho ; $[\text{Ln}(\text{H}_2\text{O})_7\{\text{X}(\text{OH})_6\text{Mo}_6\text{O}_{18}\}\text{Ln}(\text{H}_2\text{O})_7]\{\text{X}(\text{OH})_6\text{Mo}_6\text{O}_{18}\}\cdot 16\text{H}_2\text{O}$, $\text{X} = \text{Al}$ and $\text{Ln} = \text{Er, Tm}$ and Lu , $\text{X} = \text{Cr}$ and $\text{Ln} = \text{Lu}$.

EXPERIMENTAL

Selected members of the composition $[\text{Ln}(\text{H}_2\text{O})_7\{\text{X}(\text{OH})_6\text{Mo}_6\text{O}_{18}\}]\cdot 4\text{H}_2\text{O}$ and $[\text{Ln}(\text{H}_2\text{O})_7\{\text{X}(\text{OH})_6\text{Mo}_6\text{O}_{18}\}\text{Ln}(\text{H}_2\text{O})_7]\{\text{X}(\text{OH})_6\text{Mo}_6\text{O}_{18}\}\cdot 16\text{H}_2\text{O}$ have been isolated earlier by a few groups and its single crystal structures have been established (Fedoseev et al., 2002; Shivaiah et al., 2002, 2014; Gavrilova and Molchanov, 2005; Zhou and Yang, 2007; Cao et al., 2008; Shi D. et al., 2008; Shi D. M. et al., 2008; Zhang et al., 2008; Zhao et al., 2008; Wang et al., 2011; Kumar et al., 2014a). However, no group has attempted isolation of the whole series of Anderson-Evans cluster based solids containing Al or Cr heteroatoms coordinated to lanthanide cations. Two different approaches have been employed in literature to prepare the compounds: (a) Mixing aqueous solutions of pre-synthesized $\text{Na}_3\text{Cr}(\text{OH})_6\text{Mo}_6\text{O}_{18}\cdot 8\text{H}_2\text{O}$ with aqueous (or methanolic) solutions of lanthanide salts followed by heating or refluxing to 60–80°C for 30 min to 4 h after suitably adjusting pH of the reacting mixture (Zhou and Yang, 2007; Shi D. et al., 2008; Shi D. M. et al., 2008; Zhao et al., 2008; Wang et al., 2011); (b) Reacting aqueous solutions of precursor compounds for the cluster ($\text{Na}_2\text{MoO}_4\cdot 2\text{H}_2\text{O}$ and $\text{CrCl}_3\cdot 6\text{H}_2\text{O}$ or $\text{Cr}(\text{NO}_3)_3\cdot 9\text{H}_2\text{O}/\text{AlCl}_3\cdot 6\text{H}_2\text{O}$) with an acidified solution of lanthanide salts. pH of the reaction mixture was then set before keeping for solvent evaporation. In some cases the reaction mixture was refluxed at 60°C prior to solvent evaporation (Shivaiah et al., 2002, 2014; Cao et al., 2008; Kumar et al., 2014a). Our earlier experience with the synthesis of the chromium molybdate based solids (Singh et al., 2010b, 2014; Pavani et al., 2011; Singh and Ramanan, 2011; Kumar et al., 2014a) showed the quality of crystals and phase homogeneity varied considerably depending on the concentration and pH

of the reacting mixtures and the sequence of the addition of reagents. Although stoichiometry is generally the key to synthesis, in selected cases, excess or control of heteroatom concentration was found to be necessary (Pope, 1983). We also noticed that the procedures employed by other groups were limited leading to low yields and problems associated with the pre-synthesized sodium salt of Anderson-Evans cluster that resulted in competing phases driven by sodium hydrates. In aqueous solution, sodium ions are known to assemble differently with $\{\text{Cr}(\text{OH})_6\text{Mo}_6\text{O}_{18}\}^{3-}$ leading to multiple forms (Perloff, 1970; Yu et al., 2006; Singh et al., 2010b).

This led us to adopt a modified method to prepare new $\{\text{Cr}(\text{OH})_6\text{Mo}_6\text{O}_{18}\}$ based solids coordinated with transition metal ions (Singh et al., 2010b). An extension of this one-pot scheme did yield some success in isolating a few lanthanide-based chromium hexamolybdates (Kumar et al., 2014a). The method, however, was hampered to extend the series with other lanthanide ions due to the appearance of a green colored residue, possibly the formation of the solid $[\{\text{Na}(\text{H}_2\text{O})_6\}\{\text{Cr}(\text{OH})_6\text{Mo}_6\text{O}_{17}(\text{OH})\}]\cdot 24\text{H}_2\text{O}$ (Singh et al., 2010b; Pavani et al., 2011). Furthermore, these crystals started growing when the supernatant solution was left for longer time. Our initial attempts to prepare aluminum analogs led to two types of crystalline solids $[\text{Ln}(\text{H}_2\text{O})_7\{\text{Al}(\text{OH})_6\text{Mo}_6\text{O}_{18}\}]\cdot 4\text{H}_2\text{O}$ (smaller block shaped transparent crystals) and $[\text{Na}_3(\text{H}_2\text{O})_6\{\text{Al}(\text{OH})_6\text{Mo}_6\text{O}_{18}\}]\cdot 2\text{H}_2\text{O}$ (larger block shaped transparent-white crystals). To overcome these issues, we lowered the concentration of $\text{CrCl}_3\cdot 6\text{H}_2\text{O}$ and $\text{AlCl}_3\cdot 6\text{H}_2\text{O}$ and the amount of acetic acid used to adjust pH as per our previous experience. The following modified protocol has enabled us to successfully isolate almost all lanthanide-based chromium and aluminum analogs of Anderson-Evans cluster solids.

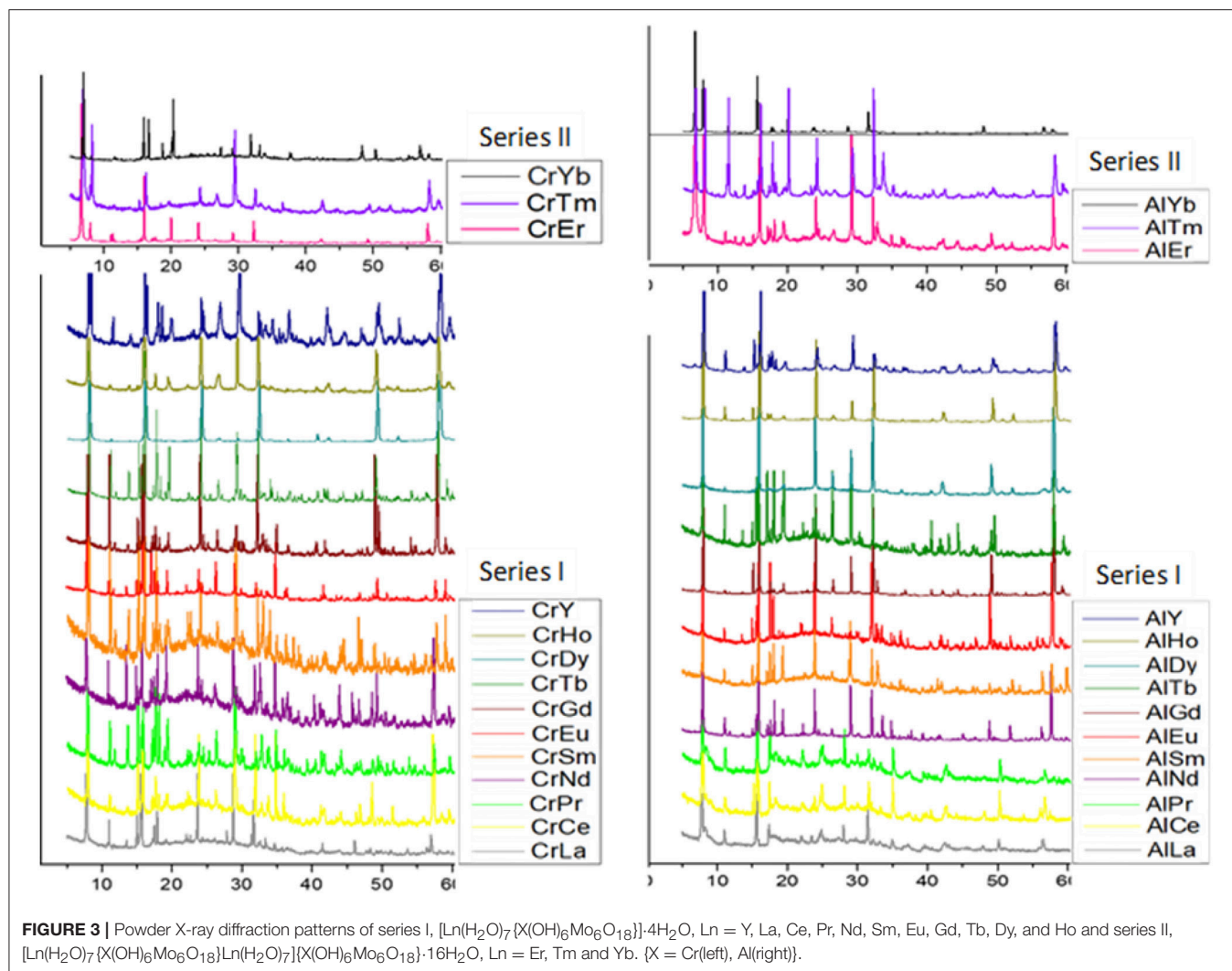
Modified synthetic protocol:

The solid $\text{AlCl}_3\cdot 6\text{H}_2\text{O}$ and all lanthanide salts (99.9% purity, trace metal basis) were purchased from Sigma Aldrich Chemicals Pvt. Ltd. (USA). $\text{Na}_2\text{MoO}_4\cdot 2\text{H}_2\text{O}$ was purchased from TCI Pvt. Ltd. and $\text{CrCl}_3\cdot 6\text{H}_2\text{O}$ was purchased from CDH Pvt. Ltd. All reagents were used without further purification. Initially, two separate solutions were prepared as per our earlier method (Singh and Ramanan, 2011).

Solution A was prepared by dissolving 0.65 mmol of $\text{Na}_2\text{MoO}_4\cdot 2\text{H}_2\text{O}$ and 0.26 mmol $\text{CrCl}_3\cdot 6\text{H}_2\text{O}/\text{AlCl}_3\cdot 6\text{H}_2\text{O}$ in 4 ml distilled water which was further acidified with 1 ml glacial CH_3COOH . **Solution B** was prepared by dissolving 0.65 mmol $\text{LnCl}_3\cdot x\text{H}_2\text{O}$ ($x = 7$ for La and Ce; $x = 6$ for Nd to Er, Yb, Lu and Y) or $\text{Ln}(\text{NO}_3)_3\cdot x\text{H}_2\text{O}$ ($x = 6$ for Pr and $x = 5$ for Tm) in 5 ml distilled water. The contents of solution A and B were mixed with continuous stirring and the resultant solution was kept at room temperature for solvent evaporation. In the case of lanthanum and cerium, crystals grew within 24 h. However, heavier lanthanides took more time to crystallize. Ytterbium crystals appeared after about 10 days.

Crystal Structures

Single crystal (Table 2) and powder X-ray diffraction analysis (Figure 3) revealed that for lighter lanthanides (till $\text{Ln} = \text{Ho}$),



Series I was observed. These solids crystallize in the space group $Pca2_1$; the cell parameters and the intensities of the reflections (**Table 1**) are comparable and in order with decreasing size of the respective ions. Of these, the compounds TbCr9, DyCr10, HoCr11, LuCr29, PrAl18, NdAl19, TbAl23, DyAl24, HoAl25, ErAl26, TmAl27, and LuAl30 are being reported for the first time. The Series II compounds ErAl26 and TmAl27 exhibited different cell parameters when loaded at low temperatures (100K). A similar observation of phase transformation in Series II type solid has been reported in the case of TmCr12 (Zhang et al., 2008). In Series I, the cluster $\{\text{X}(\text{OH})_6\text{Mo}_6\text{O}_{18}\}^{3-}$ with $\text{X} = \text{Al}$ or Cr is the basic building block and coordinates with $\{\text{Ln}(\text{H}_2\text{O})_7\}^{3+}$ to form 1D zig-zag chains (**Figure S1A**). The solids are further stabilized via nonbonding interactions with lattice water (**Figure S1B**). The bond lengths and angles are comparable to other members already known (Fedoseev et al., 2002; Shivaiah et al., 2002, 2014; Gavrilova and Molchanov, 2005; Zhou and Yang, 2007; Cao et al., 2008; Shi D. M. et al., 2008; Zhao et al., 2008; Kumar et al., 2014a). An interesting observation is that under our reaction condition yttrium analogs crystallized as Series I (**Table 1**). It is

not surprising since size of Y^{3+} in 9 CN (1.075 \AA) is comparable to 1.083 \AA of Dy^{3+} (Shannon, 1976; Lundberg et al., 2010). However, an earlier report had shown yttrium to have crystallized in Series II (Wang et al., 2011). It is clear from **Figure 3** that a transition from Series I to II, under our experimental conditions, occurs around Erbium(Er). In the case of Er, reflections clearly indicate the presence of both Series I and II. Tm also shows a concomitant mixture of the two series. However, Yb appears to be predominantly that of Series II. We strongly believe that the presence of a second phase is quite likely in all higher lanthanides and this observation is only reflected in powder XRD (**Figure 3**).

Crystallization reaction of Anderson-Evans cluster with heavier lanthanides (Er to Yb) led to Series II. These solids crystallized in $P\bar{1}$ space group (**Table 2**). Though the stoichiometry of lanthanide to the cluster in the crystal structure remained the same as in Series I, the assembly of the molecular solid (0D) was different. Also, the structure contained a larger number of uncoordinated water molecules. In Series II, the cationic cluster $[\text{Ln}(\text{H}_2\text{O})_7\{\text{X}(\text{OH})_6\text{Mo}_6\text{O}_{18}\}\text{Ln}(\text{H}_2\text{O})_7]^{3+}$ derivatised by a pair of lanthanide hydrates involved in

TABLE 1 | Refined cell parameters for solids in series I and series II.

Ln/X	Ionic radius (Ln ³⁺) in 9 and 8 CN (Å)	Series I: [Ln(H ₂ O) ₇ {X(OH) ₆ Mo ₆ O ₁₈ }]·4H ₂ O space group <i>Pca2₁</i>			
		<i>a</i> (Å)	<i>b</i> (Å)	<i>c</i> (Å)	Volume (Å ³)
YCr1#	1.075 ^a	10.889(6)	11.768(8)	22.263(13)	2853(5)
YAl1#	1.019	11.7567(8)	10.8939(7)	22.2145(15)	2845.2(3)
LaCr2	1.216 ^a	11.831(4)	10.968(4)	22.621(8)	2935(3)
LaAl16	1.160	11.844(2)	11.010(2)	22.643(5)	2952.7
CeCr3	1.196 ^a	11.777(6)	10.924(6)	22.549(11)	2901(4)
CeAl17	1.143	11.8255(15)	11.0007(14)	22.556(3)	2934.28
PrCr4	1.179 ^a	11.771(6)	10.925(5)	22.442(12)	2886(4)
PrAl18	1.126	11.8173(6)	10.9707(5)	22.5088(11)	2918.1(2)
NdCr5	1.163 ^a	11.762(5)	10.900(5)	22.425(9)	2875(3)
NdAl19	1.109	11.7659(5)	10.9321(5)	22.4151(10)	2883.2(2)
SmCr6	1.132 ^a	11.759(4)	10.921(4)	22.372(8)	2873(3)
SmAl20	1.079	11.7700(6)	10.9257(6)	22.3586(12)	2875.2(3)
EuCr7	1.120 ^a	11.778(10)	10.961(10)	22.422(19)	2895(4)
EuAl21	1.066	11.732(4)	10.909(3)	22.251(7)	2848(2)
GdCr8	1.107 ^a	11.785(3)	10.926(3)	22.349(6)	2878(2)
GdAl22	1.053	11.716(13)	10.870(12)	22.23(3)	2836(9)
TbCr9	1.095 ^a	11.8213(7)	10.9479(6)	22.3810(13)	2896.5(3)
TbAl23	1.040	11.7860(13)	10.9560(11)	22.333(2)	2883.9(5)
DyCr10	1.083 ^a	11.7813(7)	10.9100(6)	22.2821(13)	2864.0(3)
DyAl24	1.027	11.7385(5)	10.8989(5)	22.2203(10)	2842.8(2)
HoCr11	1.072 ^a	11.7696(10)	10.8829(9)	22.2283(18)	2847.2(4)
HoAl25	1.015	11.7114(11)	10.8538(10)	22.139(2)	2814.2(5)
ErCr12#	1.062 ^a	11.7799(8)	10.8875(7)	22.2105(14)	2848.6(3)
ErAl26#	1.004	11.667(18)	10.846(18)	22.11(4)	2797(8)
TmCr13#	1.052 ^a	11.7665(8)	10.8728(8)	22.2149(16)	2842.1(4)
	0.994				

Ln/X	Series II: [Ln(H ₂ O) ₇ {X(OH) ₆ Mo ₆ O ₁₈ }Ln(H ₂ O) ₇]{X(OH) ₆ Mo ₆ O ₁₈ }·16H ₂ O space group <i>P 1</i>						
	<i>a</i> (Å)	<i>b</i> (Å)	<i>c</i> (Å)	α (°)	β (°)	γ (°)	Volume (Å ³)
ErCr12	10.9762(6)	11.6149(7)	13.9397(8)	74.4390(10)	83.8050(10)	89.4570(10)	1701.65(17)
ErAl26	11.038(19)	11.067(3)	14.01(4)	74.67(10)	84.10(8)	89.41(7)	1731(10)
ErAl26*	15.5455(9)	15.8776(9)	16.0412(9)	86.9390(10)	72.4000(10)	64.5440(10)	3394.1(3)
TmCr13	11.0989(13)	11.7203(14)	13.9843(40)	74.993(2)	84.528(2)	89.545(2)	1748.9
TmAl27	10.9836(4)	11.5857(4)	13.9171(5)	74.4310(10)	83.8200(10)	89.4490(10)	1695.75(11)
TmAl27*	15.5445(12)	15.8913(12)	16.0467(12)	86.9470(10)	72.8530(10)	64.5140(10)	3396.1(4)
YbCr14	11.0379(5)	11.6436(5)	13.9044(7)	75.005(1)	84.530(1)	89.466(1)	1718.08(14)
YbAl28	11.011(10)	11.585(12)	13.885(13)	74.895(19)	84.51(2)	89.517(18)	1702(3)
YCr1	11.0492(6)	11.6488(6)	13.9350(8)	75.070(4)	84.551(4)	89.536(4)	1724.94(16)
YAl15	11.052(5)	11.620(5)	13.947(5)	75.006(5)	84.535(5)	89.582(5)	1722.0(12)

^a Ionic radii of Ln³⁺ in coordination number 9. Rest are for coordination number 8. The values are calculated from *r*³ *V* plots.

Represents the solids of series I wherein the solids of series II are also present as a concomitant phase.

complex H-bonding with another discrete anionic cluster {X(OH)₆Mo₆O₁₈}³⁻ (Figure S2). Two groups have crystallized and structurally characterized a few members belonging to Series II (Zhang et al., 2008; Wang et al., 2011). The previous works as well the present one clearly suggest that a few lattice water are disordered in solids belonging to Series II. Bond valence

sums conclusively show that lanthanide, chromium/aluminum and molybdenum occur in +3, +3, and +6 oxidation state, respectively.

A close inspection of the structures, however revealed that the crystal packing of the complex cation, and the discrete anion, showed a strong resemblance to Series I (Figures 4A,C).

TABLE 2 | Crystal data and refinement details for all single crystals reported for the first time.

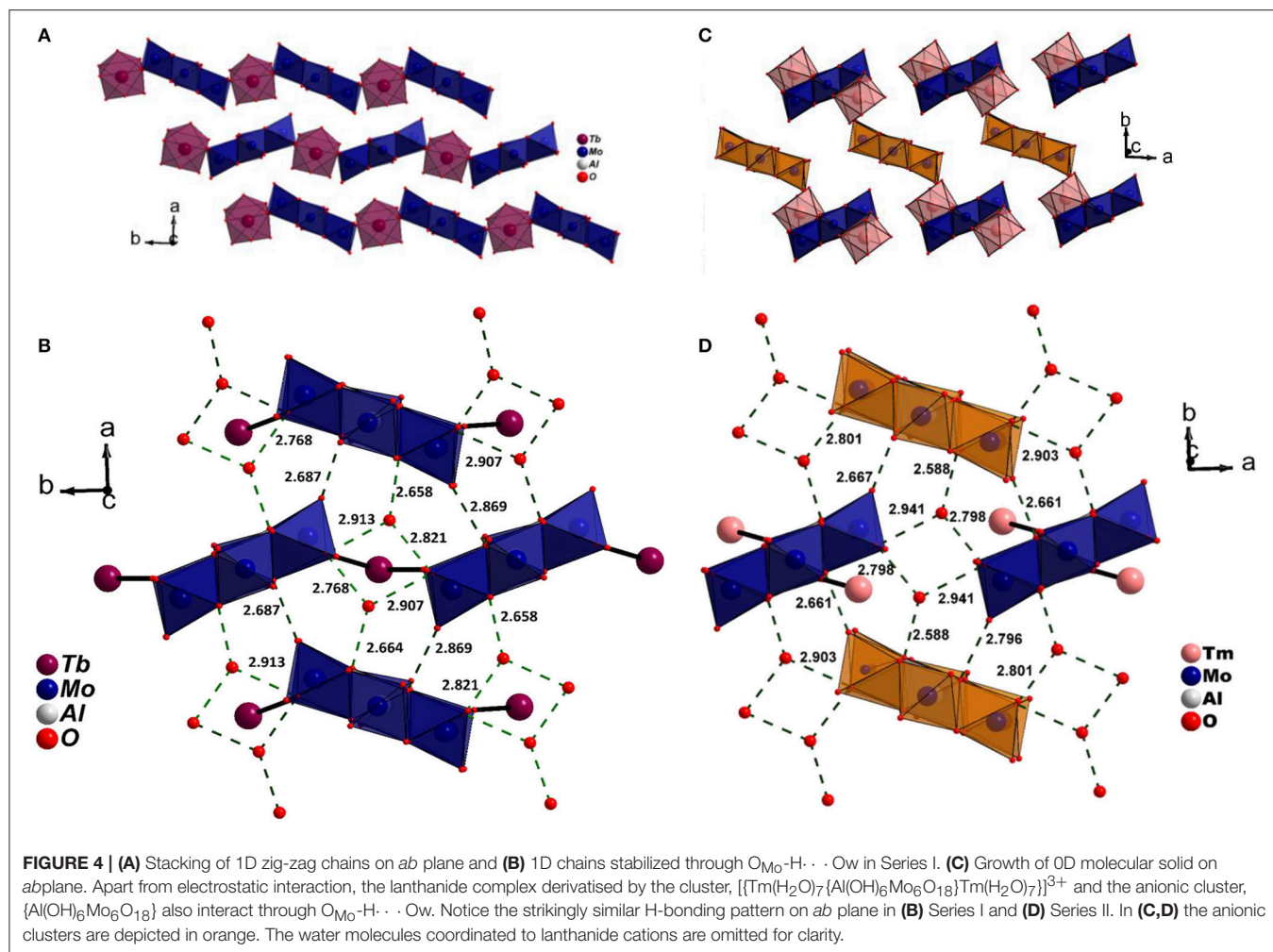
Parameter	TbCr9	DyCr10	HoCr11	ErCr12#	TmCr13#	LuCr29	PrAl18	NdAl19	TbAl23
Formula	Cr ₂ Mo ₁₂ O ₇₀ Tb ₂	Cr ₂ Dy ₂ Mo ₁₂ O ₇₀	Cr ₂ Ho ₂ Mo ₁₂ O ₇₀	Cr ₂ Er ₂ Mo ₁₂ O ₇₀	Cr ₂ Mo ₁₂ O ₇₀ Tm ₂	Cr ₂ Mo ₁₂ O ₇₈ Lu ₂	Al ₂ Mo ₁₂ O ₇₀ Pr ₂	Al ₂ Mo ₁₂ Nd ₂ O ₇₀	Al ₂ Mo ₁₂ O ₇₀ Tb ₂
Formula weight	2,693.14	2,732.28	2,705.14	2,741.80	2,713.14	2,853.22	2,607.06	2,613.72	2,643.10
T (K)	298(2)	100(2)	100(2)	100(2)	100(2)	298(2)	298(2)	100(2)	298(2)
Crystal system	Orthorhombic	Orthorhombic	Orthorhombic	Orthorhombic	Orthorhombic	Triclinic	Orthorhombic	Orthorhombic	Orthorhombic
Space group	<i>Pca</i> 2 ₁	<i>P</i> $\bar{1}$	<i>Pca</i> 2 ₁	<i>Pca</i> 2 ₁	<i>Pca</i> 2 ₁				
<i>a</i> (Å)	11.8213(7)	12.0050(7)	11.8069(12)	11.7799(8)	11.7665(8)	11.0470(2)	11.8173(6)	11.7210(6)	11.7860(13)
<i>b</i> (Å)	10.9479(6)	11.0090(6)	10.9263(11)	10.8875(7)	10.8728(8)	11.6690(2)	10.9707(5)	10.8990(5)	10.9560(11)
<i>c</i> (Å)	22.3810(13)	22.660(13)	22.2930(2)	22.2105(14)	22.2149(16)	13.9150(3)	22.5088(11)	22.3370(11)	22.3330(2)
α (°)	90	90	90	90	90	74.937(4)	90	90	90
β (°)	90	90	90	90	90	11.669(2)	90	90	90
γ (°)	90	90	90	90	90	13.915(3)	90	90	90
<i>V</i> (Å ³)	2,896.5(3)	2,864.0(3)	2,875.9(5)	2,848.6(3)	2,842.1(4)	1,724.0(6)	2,918.1(2)	2,853.2(2)	2,883.9(5)
<i>Z</i>	2	2	2	2	2	1	2	2	2
Dcalc (gcm ⁻³)	3.086	3.006	3.161	3.197	3.170	2.748	2.967	3.042	3.044
$\mu_{\text{Mok}\alpha}$ (cm ⁻¹)	5.402	5.320	5.737	5.961	6.139	5.365	4.286	4.494	5.100
Theta range (°)	2.60–31.31	2.50–35.50	2.54–24.57	2.55, 26.44	2.55–28.54	2.51–30.75	2.53–30.44	2.62–31.30	2.54–31.05
R ₁ , wR ₂ [<i>I</i> > 2 σ (<i>I</i>)] ^a	0.0484, 0.1236	0.0744, 0.1985	0.0623, 0.1364	0.0799, 0.1603	0.0695, 0.1964	0.0510, 0.1477	0.0309, 0.0901	0.0442, 0.1051	0.0606, 0.1488
GOF	1.022	1.539	1.064	1.164	1.619	1.275	0.786	0.853	1.088
ICSD no.	1881544	1821829	1881881	1881880	1881833	1881617	1881543	1881610	1881555

Parameter	DyAl24	HoAl25	ErAl26#	ErAl26*	TmAl27	TmAl27*	LuAl30
Formula	Al ₂ Dy ₂ Mo ₁₂ O ₇₀	Al ₂ Ho ₂ Mo ₁₂ O ₇₀	Al ₂ Mo ₁₂ Er ₂ O ₇₀	Al ₂ Er ₂ Mo ₁₂ O ₇₈	Al ₂ Mo ₁₂ O ₇₈ Tm ₂	Al ₂ Mo ₁₂ Tm ₂ O ₇₈	Al ₂ Mo ₁₂ Lu ₂ O ₇₈
Formula weight	2,650.24	2,687.10	2,693.14	2,803.76	2,803.20	2,791.10	2,803.18
T (K)	100(2)	100(2)	100(2)	100(2)	100(2)	100(2)	298(2)
Crystal system	Orthorhombic	Orthorhombic	Orthorhombic	Triclinic	Triclinic	Triclinic	Triclinic
Space group	<i>Pca</i> 2 ₁	<i>Pca</i> 2 ₁	<i>Pca</i> 2 ₁	<i>P</i> $\bar{1}$	<i>P</i> $\bar{1}$	<i>P</i> $\bar{1}$	<i>P</i> $\bar{1}$
<i>a</i> (Å)	11.7385(5)	11.7114(11)	11.667(18)	15.5455(9)	11.0276(7)	15.5445(12)	11.0453(14)
<i>b</i> (Å)	10.8989(5)	10.8538(10)	10.846(18)	15.8776(9)	11.5944(7)	15.8913(12)	11.6203(14)
<i>c</i> (Å)	22.2203(10)	22.1390(2)	22.110(4)	16.0412(9)	13.8969(9)	16.0467(12)	13.8854(17)
α (°)	90	90	90	86.9390(10)	74.981(2)	86.947(1)	74.975(2)
β (°)	90	90	90	72.4000(10)	84.559(2)	72.358(1)	84.571(2)
γ (°)	90	90	90	64.5440(10)	89.539(2)	64.514(1)	89.568(2)
<i>V</i> (Å ³)	2,842.8(2)	2,814.2(4)	2,797.0(8)	3,394.1(3)	1,708.15(19)	3,396.1(4)	1,713.3(4)
<i>Z</i>	2	2	2	2	1	2	1
Dcalc (gcm ⁻³)	3.096	3.133	3.157	2.740	2.725	2.730	2.717
$\mu_{\text{Mok}\alpha}$ (cm ⁻¹)	5.314	5.524	5.728	4.738	4.847	4.876	5.124
Theta range (°)	2.55–30.74	2.56–20.92	2.55–27.27	2.28–30.75	2.29–29.09	2.58–30.92	2.51–30.86
R ₁ , wR ₂ [<i>I</i> > 2 σ (<i>I</i>)] ^a	0.0308, 0.0765	0.0571, 0.1415	0.1078, 0.1693	0.0435, 0.1086	0.0557, 0.1000	0.0787, 0.3366	0.0310, 0.1056
GOF	1.020	1.055	1.196	1.027	1.047	2.413	0.861
ICSD no.	1881556	1881882	1881830	1881609	1881832	1881834	1881831

Represents the solids of series I wherein the solids of series II are also present as a concomitant phase.

It is important to point out that the non-bonding interactions of the two series on the *ab* plane are strikingly similar (Figures 4B,D) signifying the small energy difference between the two supramolecular aggregates. However, since higher lanthanides favor a lower coordination number due to smaller size, an extended chain appears to be unfavorable. Interestingly, Ln³⁺ coordinates to terminal oxygen (O_t) of the hexagonal cluster at 1,4 positions (Series II) in contrast to 1,3 found in

Series I (Figures S1, S2). An efficient close packing probably necessitates the formation of a complex cation wherein the cluster is coordinated by a pair of [Ln(H₂O)₇]³⁺ via symmetry equivalent terminal oxygen atoms. As a consequence, the complex cations and anions stack one over the other in a twisted fashion (Figure 5). The packing is further facilitated by non-bonding interactions with additional water molecules that get incorporated into the structure. The present study as well as

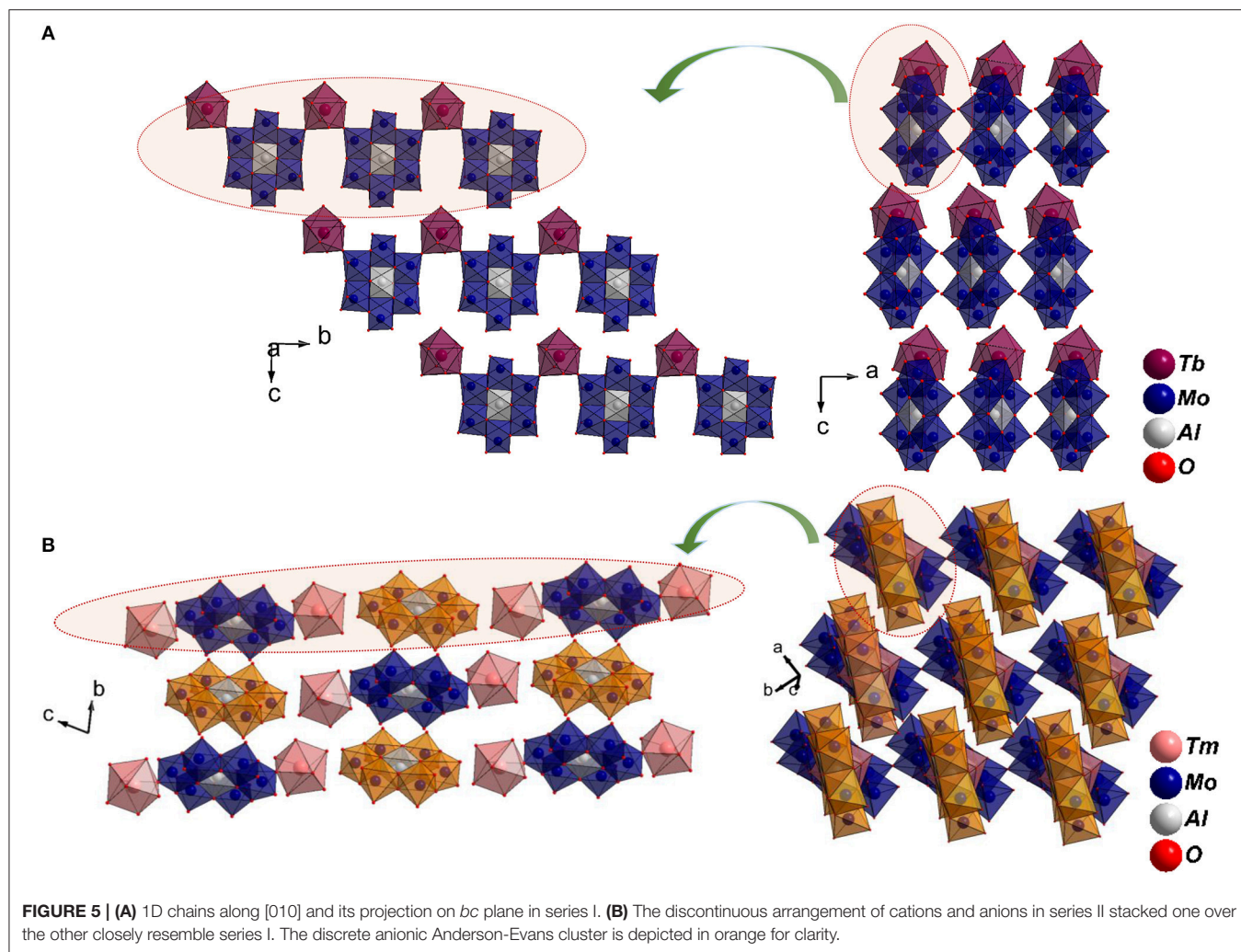


the two literature reports clearly show that the occurrence of a significant disorder among lattice water thus making it difficult to obtain a reliable model.

Crystallization of Lanthanide Coordinated Chromium/Aluminum Molybdates

A molybdenum source dissolved in aqueous medium under varying concentration and *pH* may contain numerous soluble molybdate species (Tkac and Paulenova, 2008). Under our experimental conditions, it is reasonable to assume the occurrence of stable Anderson-Evans cluster (Pavani et al., 2011). Crystallization is a supramolecular reaction (Desiraju, 2007; Singh et al., 2010a; Desiraju et al., 2011; Singh and Ramanan, 2011) and hence a crystal separating from a medium can be considered to occur from the aggregation of appropriate molecular species including solvent molecules. In the context of crystal engineering of lanthanide coordinated with chromium or aluminum molybdate cluster, two species, *viz.* $\{Ln(H_2O)_n\}^{3+}$ and $\{X(OH)_6Mo_6O_{18}\}^{3-}$ aggregate along with water molecules leading to a stable crystal, belonging to Series I or II (Singh et al., 2010b, 2014; Pavani et al.,

2011; Singh and Ramanan, 2011; Kumar et al., 2014b). In Series I, the cations and anions condense forming extended chains through coordination linkages whereas in Series II, the smaller size of lanthanides results in the formation of a discrete cationic complex wherein the cluster is coordinated by a pair of lanthanide ions. The packing of the cations and the discrete cluster anions are facilitated through nonbonding interactions and hence more water molecules get incorporated into the structure. The two closely related isostructural series represent an intriguing example of crystal engineering of salt hydrates manifested by parsimonious nature to compromise between Kitaigorodskii's close packing principle (Kitaigorodskii, 1965) and non-covalent interactions assembling into a stable crystal under a given condition. The principle appears to be the same operating in a simple salt hydrate crystallizing from a supramolecular assembly of water-mediated $\{Cu(H_2O)_6\}^{2+}$ and SO_4^{2-} leading to 0D (molecular) $CuSO_4 \cdot 7H_2O$ (Boothite), 1D (chain) $CuSO_4 \cdot 5H_2O$ (Chalcantite) and multidimensional $CuSO_4 \cdot 3H_2O$ (Bonattite), $CuSO_4 \cdot H_2O$ (Poitevinte) and $CuSO_4$ (Chalcocyanite) or organic hydrates (Upreti et al., 2007; Singh et al., 2010a).



Excitation and Emission Spectra of Rare-Earth Chromium/Aluminum Molybdates

Till recently there are only five papers that have reported emission (PL) of solids containing lanthanides and chromium molybdate cluster (Yusov et al., 2002; Cao et al., 2008; Shi D. M. et al., 2008; Yang et al., 2013; Kumar et al., 2014a). Generally, polycrystalline samples may be contaminated and are prone to react with air. In this work, we carried out PL studies directly on single crystals. Microscopic PL spectra and images are obtained from a modified microscope. Both excitation (PLE) and emission (PL) studies were conducted on commercial spectrofluorophotometer (see Experimental section). As visible to naked eye, all rare-earth containing chromium molybdate crystals ($\text{Ln} = \text{La}, \text{Ce}, \text{Pr}, \text{Nd}, \text{Sm}, \text{Eu}, \text{Gd}, \text{Tb}, \text{Dy}, \text{Ho}, \text{Er}, \text{Tm}, \text{Yb}, \text{and Y}$) exhibit strong reddish-purple emission. In **Figure 6**, we have shown emission spectra of all the rare-earth containing chromium molybdate solids (refer also **Figure S10**). This is to be noted that only Sm, Eu, Tb, and Dy are known to show strong emission in the visible region. The corresponding aluminum

analog (**Figure 6**) showed only characteristic emission from the respective lanthanide ions. In general, lanthanides are prone to give strong discrete emission due to *f-f* transitions, whereas Cr^{3+} is from *3d* band contribution. The domination of Cr^{3+} emission from the lanthanide containing chromium molybdates still remains an intriguing problem. Europium doped solids (crystalline phosphors and glasses) strongly emitting in orange-red region are known structural probes for identification of symmetry and coordination (Swapna et al., 2014). To analyze further, we recorded PL spectra of EuCr_7 at various excitation levels of both Cr^{3+} and Eu^{3+} transitions (**Figure 7**). For all excitation energies, we observed only signatures of Cr^{3+} ion, occurring at around 692, 709 and 733 nm attributed to Stokes shifted ${}^2T_1 \rightarrow {}^4A_2$ (R-lines) and ${}^2E \rightarrow {}^4A_2$ transitions. It is widely accepted that Cr^{3+} ion emission is highly dependent on temperature and on the matrix in which the ion is situated. The sharp emission around 703 and 704.4 nm observed for Cr^{3+} in $[\text{Na}_3\{\text{Cr}(\text{OH})_6\text{Mo}_6\text{O}_{18}\} \cdot 8\text{H}_2\text{O}]$ at 4.2 K was assigned to R-lines (Yamase and Sugeta, 1993). Similar to our earlier observation (Kumar et al., 2014a), the room-temperature spectra of all chromium molybdates showed only the dominant red

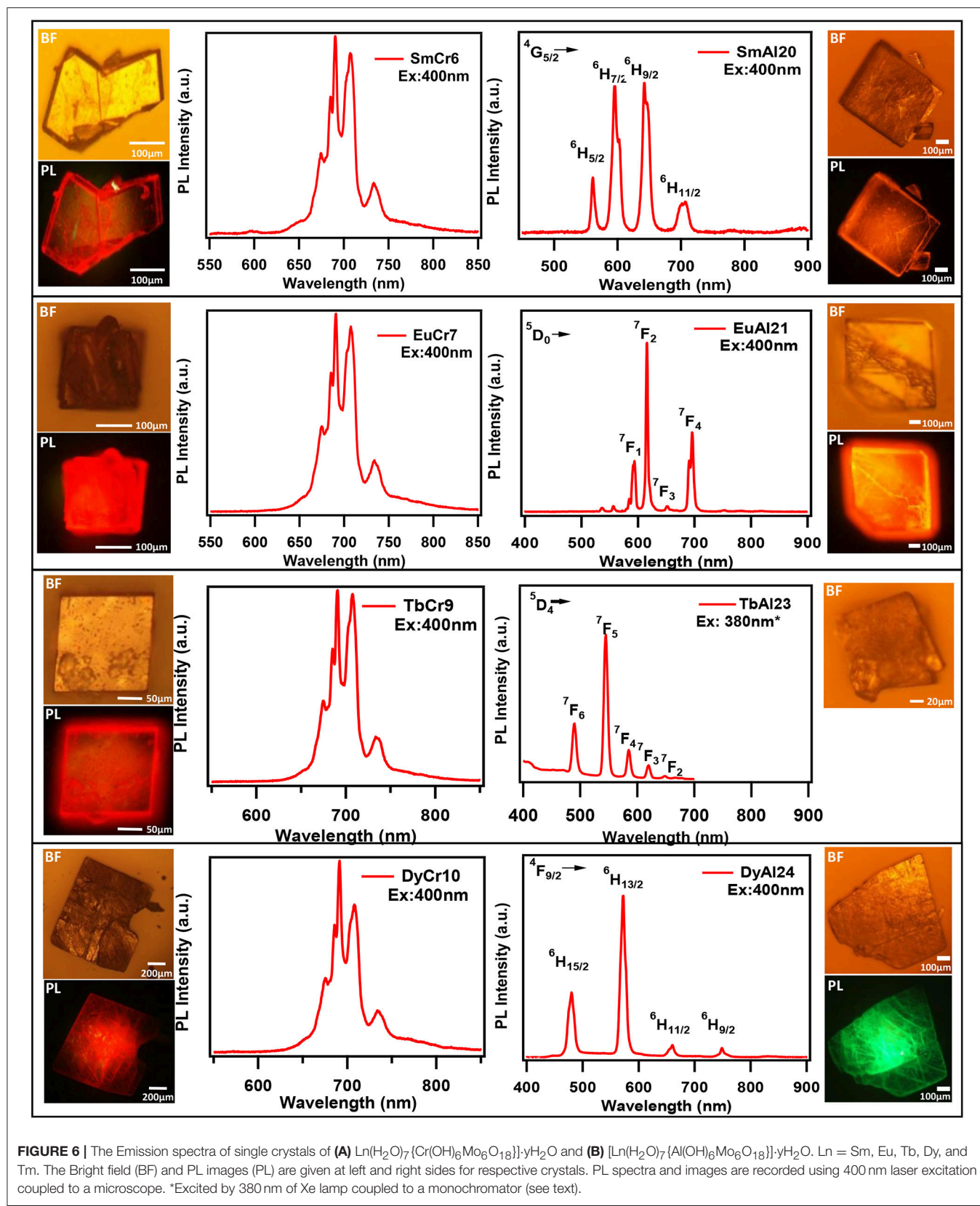
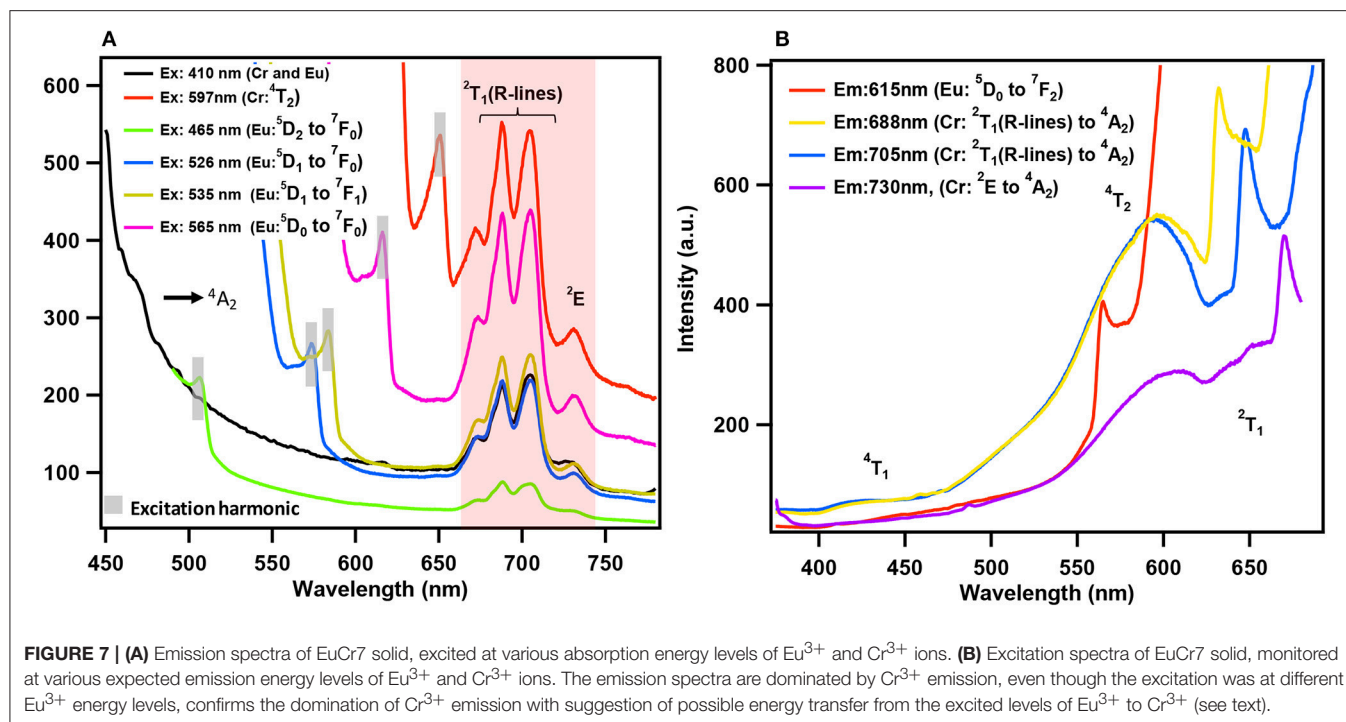


FIGURE 6 | The Emission spectra of single crystals of (A) $\text{Ln}(\text{H}_2\text{O})_7[\text{Cr}(\text{OH})_6\text{Mo}_6\text{O}_{18}]\cdot y\text{H}_2\text{O}$ and (B) $[\text{Ln}(\text{H}_2\text{O})_7[\text{Al}(\text{OH})_6\text{Mo}_6\text{O}_{18}]]\cdot y\text{H}_2\text{O}$. Ln = Sm, Eu, Tb, Dy, and Tm. The Bright field (BF) and PL images (PL) are given at left and right sides for respective crystals. PL spectra and images are recorded using 400 nm laser excitation coupled to a microscope. *Excited by 380 nm of Xe lamp coupled to a monochromator (see text).



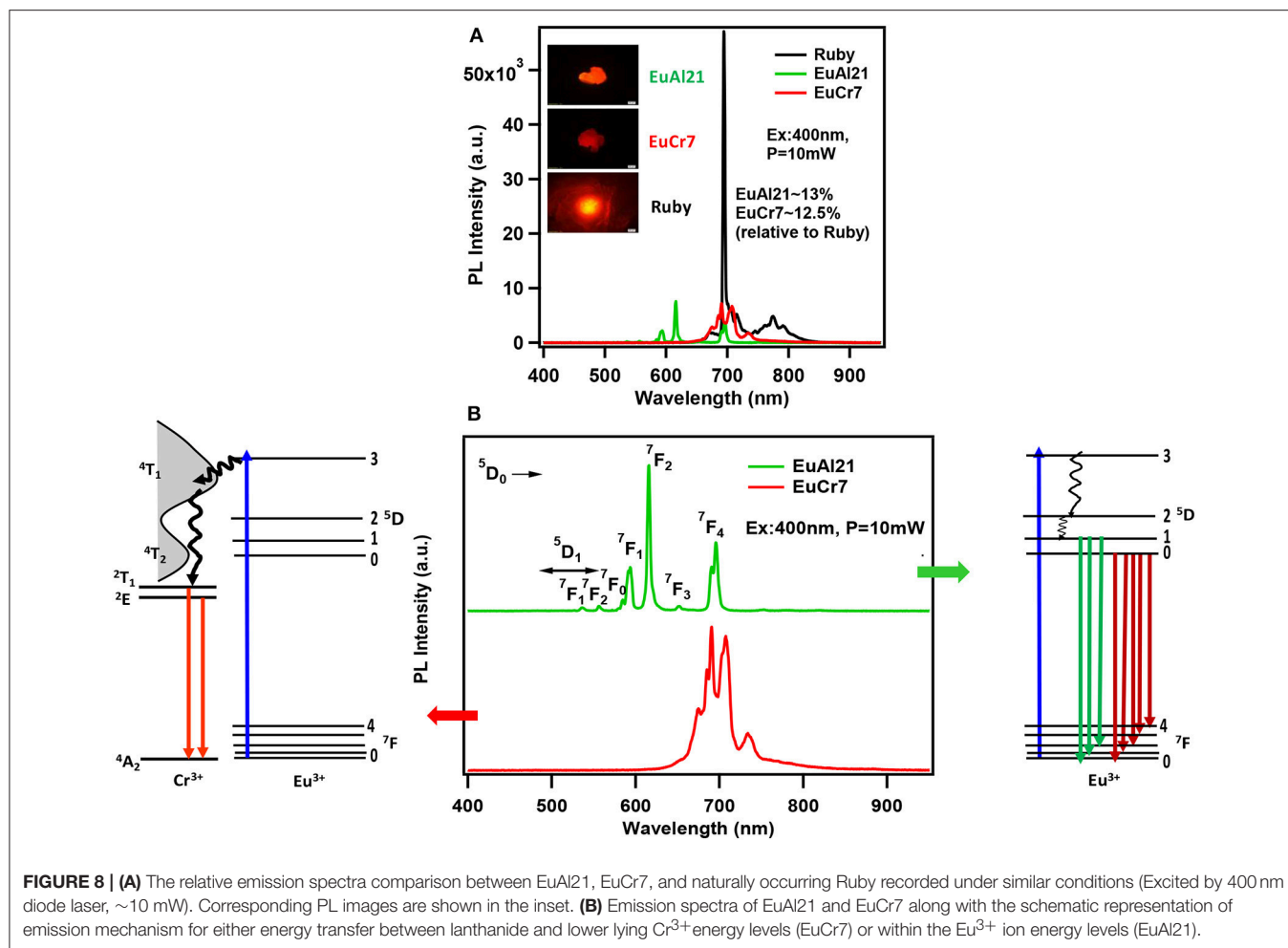
emission (Figure 6). The purple color strikingly visible to naked eye suggests that non-radiative processes leading to low emission quantum yield of R-lines is unlikely.

The excitation (PLE) spectra at the prominent emission lines of Cr^{3+} and Eu^{3+} ions (Figure 7) observed at 423, 581 and 648 nm correspond to absorption transitions of Cr^{3+} in pseudo-octahedral geometry, ${}^4\text{A}_2 \rightarrow {}^4\text{T}_1$ (F), ${}^4\text{T}_2$, and ${}^2\text{T}_1$. Therefore, it is convenient to conclude that the observed emission in EuCr7 and other chromium analogs is essentially from Cr^{3+} without any traces of contribution from the optically active lanthanide ions. PLE and PL spectra shown in Figure 7, categorically confirms the domination of Cr^{3+} emission suggesting a possible energy transfer from excited levels of Eu^{3+} to Cr^{3+} . Figure 8, shows a comparison of relative emission intensities of EuCr7 and EuAl21 single crystals, along with natural ruby crystal. The experiments are conducted under identical condition (same excitation power densities, integration time etc). The relative PL intensities and profile broadly suggest dominance of Cr^{3+} emission from EuCr7 and characteristic emission of Eu^{3+} from EuAl21. The relative intensities of both solids are about 13% on comparison with the natural ruby. Therefore, in EuCr7 it may be concluded that while excited by 400 nm (${}^5\text{D}_3$ level of Eu^{3+}) (or any other transitions of ${}^5\text{D}_j$ ($j = 0, 1, 2$) levels), the excited densities are completely energy transferred to the equivalent energy bands of ${}^4\text{T}_1$ and ${}^4\text{T}_2$, then depopulates radiatively from ${}^2\text{T}_1$ and ${}^2\text{E}$ to ground state ${}^4\text{A}_2$ of Cr^{3+} ion. On the other hand, EuAl21 solid, the excitation to until ${}^5\text{D}_0$ level, results into the emission from ${}^5\text{D}_1$ to ${}^7\text{F}_j$ ($j = 0, 1, 2$) and ${}^5\text{D}_0$ to ${}^7\text{F}_j$ ($j = 0, 1, 2, 3, 4$) of Eu^{3+} ion. The schematic energy levels of EuCr7 and EuAl21 are given in Figure 8.

It is to be noted that the absence of Eu^{3+} emission and the presence of ruby-like emission (at 77 K) in

$[\text{Eu}(\text{H}_2\text{O})_7\{\text{Cr}(\text{OH})_6\text{Mo}_6\text{O}_{18}\}]$ was also observed previously by another group (Yusov et al., 2002). Surprisingly, two solids reported in the literature have exhibited contrasting results. $[\text{Eu}(\text{H}_2\text{O})_7\{\text{Cr}(\text{OH})_6\text{Mo}_6\text{O}_{18}\}] \cdot 4\text{H}_2\text{O}$ (Shi D. M. et al., 2008) showed only characteristic emission due to Eu^{3+} ions with no trace of Cr^{3+} emission. Similarly, the molecular solid $[(\text{C}_6\text{H}_5\text{NO}_2)_2\{\text{Dy}(\text{H}_2\text{O})_6\}\{\{\text{Cr}(\text{OH})_6\text{Mo}_6\text{O}_{18}\}\}] \cdot 2(\text{C}_6\text{H}_5\text{NO}_2) \cdot 6\text{H}_2\text{O}$ also showed characteristic emission only from Dy^{3+} ion (Yang et al., 2013). It can be argued that in the latter solid, there is no direct coordination linkage between the lanthanide and the cluster. However, another molecular solid, $[(\text{Hbipy})_2\{\{\text{Cr}(\text{OH})_6\text{Mo}_6\text{O}_{17}(\text{OH})\}\}]$ displayed typical Cr^{3+} emission only (Li et al., 2016). Therefore, having the extensive experimental evidence from the present study, the suppression of lanthanide emission and dominant chromium emission could be attributed to strong absorption cross-section of Cr^{3+} ions and energy transfer (ET) between $4f-4f$ emission transitions of Ln^{3+} ions to that of $\text{Cr}^{3+}d$ -orbital energy levels. While all the compounds showed bright red emission, in the special case of NdCr5, the red emission from Cr^{3+} is considerably quenched. Figure S8 shows a comparison of the same with EuCr7, recorded under similar condition, along with PL images. It can be speculated that Cr^{3+} emitting energy level ${}^2\text{E}$ is closer to Nd^{3+} level ${}^4\text{F}_{3/2}$, therefore the quenching of emission intensity may be possible (Weber, 1973); However, further studies are required to address this issue.

One of the characteristic features of a trivalent lanthanide ion is the strong and sharp $4f$ shell absorption and emission peaks that cover a wide range of spectral regions, from UV to IR. It is known that the lanthanide $4f-4f$ transition strengths and positions are sensitive to the local environment within



a crystalline network. PL studies of the aluminum analogs (Figure 6) revealed that the solids containing Sm, Eu, and Dy ions exhibited characteristic emission as expected (de Bettencourt-Dias, 2014). In Table 3, we have also shown the excitation and emission spectra with corresponding assignments. The visible emitting TbAl23 excitation and emission spectra are given in Table 3 and Figure S7. Since Tb³⁺ does not have any energy level corresponding to the diode laser excitation source (400 nm), the microscopic PL spectra and images could not be obtained in Figure 6. The aluminum analogs of Ce³⁺, Pr³⁺, Ho³⁺, and Er³⁺ compounds did not show any appreciable PL in the visible region while excited in the UV- blue region. Another UV-violet low emitting solid TmAl27 and Cr³⁺ emission dominated TmCr13 PL spectra are shown in Figure S8.

PHYSICAL MEASUREMENTS

Single-Crystal X-ray Diffraction

Data collections were performed on a Bruker D8-Quest diffractometer with a Turbo X-ray Source (MoK α radiation, $\lambda = 0.71073 \text{ \AA}$) adopting the direct drive rotating anode technique and a PHOTON detector. The data frames were collected using the program APEX3 and processed using the program SAINT

routine in APEX3. The structures were solved by direct methods and refined by the full-matrix least-squares on F^2 using the SHELXTL-2014 program.

Powder X-ray Diffraction

Room temperature powder X-ray diffraction data (PXRD) were collected on a Bruker D8 Advance diffractometer using Ni-filtered CuK α radiation employing a step size of 0.02 and at count time of 1 s per step over the range $5^\circ < 2\theta < 80^\circ$. Rietveld refinement of powder diffraction data of all polycrystalline samples were carried out using Topas 4.2, Bruker for ensuring homogeneity of the synthesized products (Table S1).

Optical Measurements

Visible emission (~400–700 nm) and excitation spectra (300–520 nm) were recorded using a Spectrofluorophotometer (Shimadzu RF-5301PC), where the Xenon lamp is used as light source (Figure 6 and Table 3). The microscopic optical images (Bright field), PL images and visible emission spectra were recorded using a modified confocal high-resolution microscope (Olympus BX-51) (Figures 6–8). The modified microscope is equipped with a fiber coupled 400 nm (± 5 nm) diode laser and xenon lamp as sources. The emission spectra and images were

TABLE 3 | Excitation and emission spectra of optically active lanthanides along with corresponding energy levels of Sm, Eu, Tb, and Dy. All the spectra are taken by a spectrofluorophotometer utilizing xenon lamp (see text). All assigned transitions (in parenthesis) are as per the reference (de Bettencourt-Dias, 2014).

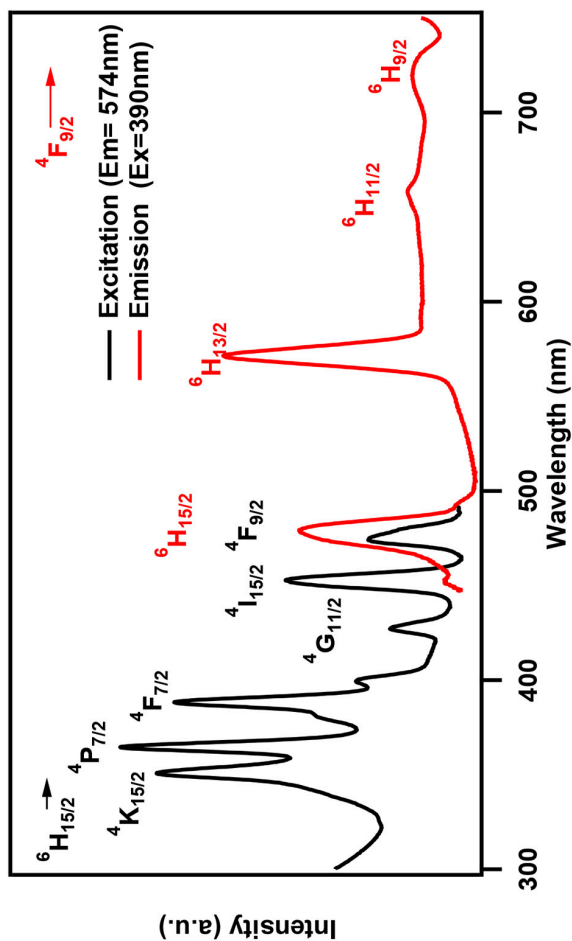
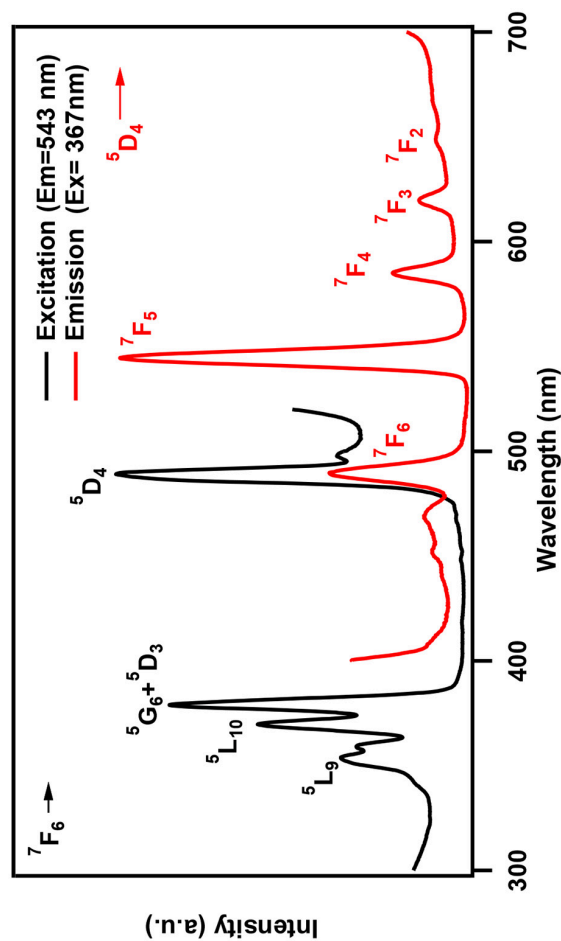
Ln ⁺³	Emission transitions		
	Excited state	Ground state	Wavelength (nm)
Sm	$^4G_5/2$	$^6H_5/2$	560 (560)
		$^6H_7/2$	595 (595)
		$^6H_9/2$	642 (640)
		$^6H_{11/2}$	720 (700)
Eu	5D_1 5D_0	7F_0	525 (525)
		7F_1	535 (530)
		7F_2	555 (560)
		7F_0	583 (583)
		7F_1	592 (590)
		7F_2	615 (615)
		7F_3	650 (650)
		7F_4	694 (720)

(Continued)

TABLE 3 | Continued

Ln ³⁺	Emission transitions		
	Excited state	Ground state	Wavelength (nm)
Tb	⁵ D ₄	⁷ F ₆	490 (490)
		⁷ F ₅	545 (540)
		⁷ F ₄	585 (580)
		⁷ F ₃	620 (620)
		⁷ F ₂	648 (650)

Excitation and emission spectra



collected, respectively by a fiber optic spectrometer (Ocean Optics, Maya 2000Pro) and a camera (Olympus, DP26) through a 425 nm long-pass filter (Pradeesh et al., 2009; Optics Express) in specular reflection mode.

Vibrational Spectroscopy

FT-IR was recorded on a Nicolet 5DX spectrophotometer with pressed KBr pellets in the range of 4,000–400 cm^{-1} . All the peaks are consistent with literature reports (Fedoseev et al., 2002; Bridgeman, 2006; Kumar et al., 2014a) (Figures S2A–X, S3A–D). The broad peaks at 3,500–3,200 cm^{-1} correspond to the O–H bond stretch. Due to differently bound water molecules, there is an observable splitting of these bands. The peaks at 1,630–1,620 cm^{-1} are characteristic of the deformation vibrations of H–O–H owing to the presence of coordinated and lattice water molecules. A peak at about 1,400 cm^{-1} in the case of Pr is observed, which has been reported by another group, which could not be explained adequately (Fedoseev et al., 2002). The low wavenumber peaks (960–400 cm^{-1}) are alike and are characteristic of the Anderson-Evans cluster. The bands at 950–890 cm^{-1} correspond to the symmetric stretching frequencies of the Mo–O_t bonds. The shape and intensity of the peaks are not sensitive to the nature of both the lanthanide and the cluster. The bands due to the vibrations of the bridging Mo–O–Mo bonds of different types are observed in the 700–400 cm^{-1} region. The replacement of the larger Cr³⁺ ion by Al³⁺ results in a noticeable shift of the vibrations of Mo–O–Mo from ~460–440 in case of Al to ~410–420 cm^{-1} in case of Cr.

Thermal Studies

Thermogravimetric analysis for selected solids were carried out using a Perkin-Elmer TGA7 system on well ground samples under a flowing nitrogen atmosphere with a heating rate of 10°C min⁻¹ in the range 40–800°C. The weight loss is almost consistent throughout the scan making it difficult to assign loss in steps. The presence of concomitant phases in the heavier lanthanides (Er and Tm) also makes it difficult to assign weight loss appropriately (Figures S3A–H).

As expected, thermal behavior of the two series (I and II) of solids were slightly different. For series I, the first weight loss (11–13%) occurred in the range of 40–120°C corresponding to the four lattice and two coordinated water. The slope of the curve clearly suggests the instability of an expected intermediate phase, [Ln(H₂O)₇{X(OH)₆Mo₆O₁₈}]_γ. The second weight loss of about 5–6% in the range of 150–330°C possibly corresponds to the loss of remaining coordinated water molecules. The total weight loss ~18–20% till ~500°C was in good agreement with complete decomposition of the solids to the respective oxides including the loss of hydroxyl groups attached to the cluster. For series II, the first weight loss (40–170°C) of about 10–11% corresponds to the loss of sixteen water molecules while the second one (170–320°C) about 9–10% correspond to the loss of fourteen coordinated water molecules. It is to be noted that for Er and Tm, the total weight loss showed significant deviation. This can be ascribed to the presence of a mixture of series I and II. Our TGA results are comparable to the earlier reports (Cao et al., 2008; Shi D. M. et al., 2008; Zhang et al., 2008; Wang et al., 2011).

CONCLUSIONS

Our strategy to assemble Anderson-Evans cluster and lanthanide hydrate through a one-pot synthesis led to two closely related structures of the composition [Ln(H₂O)₇{X(OH)₆Mo₆O₁₈}]_γH₂O (X = Cr or Al). The lighter lanthanide ions (till Ho³⁺) favored extended lanthanide cluster coordination interaction forming 1D chains, while the heavier ones (Er and above) resulted in a stacking of a cation, Anderson-Evans cluster derivatised by a pair of lanthanide hydrates and an anion, a discrete Anderson-Evans clusters through H-bonding (0D). In both series, lattice water provides further stability to the structure. Observation of purple color in all chromium molybdate cluster based solids reported here as well as in literature is attributed to the domination of Cr³⁺ emission. Quenching of lanthanide emission in rare-earth coordinated chromium based Anderson-Evans cluster can be ascribed to energy transfer from 4f levels of Ln³⁺ ions to that of Cr³⁺ d-orbital energy levels. Further theoretical calculations are required to quantify the same. A future problem is to extend our methodology to assemble aluminum based cluster anion with two or more emitting lanthanide ions, i.e., possible solid solutions to realize white light materials. The paper highlights that structure-property evaluation of a POM system is more meaningful toward the design of functional materials if one adopts a crystal engineering approach to rationalize the fundamental chemistry.

AUTHOR CONTRIBUTIONS

AR conceived the idea as he has been working in this field for over 20 years. ST has the lead role in designing the synthesis and characterization. B and VK helped in the refinement crystal structures and supported in data collection and analysis. GJ supported in synthesis and data collection. MA carried out the photoluminescence experiments and related tasks. GVP carried out the photoluminescence studies and related tasks.

FUNDING

ST and AR acknowledge SERB (EMR/2016/004021) for a research fellowship and financial support. AR acknowledges DST: SR/FST/CSII-07/2014) for funding the single crystal diffractometer to the Chemistry Department, IIT Delhi.

ACKNOWLEDGMENTS

We thank both reviewers for their critical comments and suggestions to improve the manuscript. We thank Professor J. J. Vittal (NUS, Singapore) and Dr. B. Sridhar (IICT, Hyderabad) for their help in modeling the disordered water molecules of Series II. We are thankful to Mr. Sami Makki, M/s. Matrix India for gifting native ruby crystals. We also thank Ms. Manisha Jadon and Ms. Bharti Singh for help with various measurements.

SUPPLEMENTARY MATERIAL

The Supplementary Material for this article can be found online at: <https://www.frontiersin.org/articles/10.3389/fchem.2018.00631/full#supplementary-material>

In Supplementary Material, **Table 1** contains crystallographic information files (CIF) for all unreported solids, their Rietveld refinement plots (**Figure S3**), IR plots for all the synthesized solids (**Figures S4, S5**), Thermal Analysis plots for selected solids (**Figure S6**), Emission spectra of TbAl23 from commercial spectrofluorophotometer (**Figure S7**), the emission spectra for TmCr13 and TmAl27 is given in **Figure S8**. Figure S9 shows the emission comparison of EuCr7 and NdCr5. The emission spectra of other Cr-based solids and their corresponding Bright Field and

Photoluminescence images are shown in **Figure S10**. Rietveld refined parameters of all unreported solids (**Table S1**). **Table S2** has crystal structure and refinement parameters of reported solids that were resynthesized. IR frequencies (**Table S3**). Bond Valance Sum calculations for TbAl23 and TmAl27 (**Table S4**). **Table S5** contains the yields for all solids synthesized and **Table S6** reports selected bond distances and angles for all unreported solids. Optical data for all solids (**Figures 4, S10**). **Image 1** contains the **Graphical Abstract** which shows pictures of all the solids prepared for this study taken from Nikon D3300 DSLR camera (middle) and Nikon SMZ-745T microscope (top and bottom). A clear pink color is visible to eye can be seen in chromium analogs whereas in aluminum analogs, the typical color of corresponding lanthanides can be seen.

REFERENCES

- Ai, H., Wang, Y., Li, B., and Wu, L. (2014). Synthesis and characterization of single-side organically grafted Anderson-type polyoxometalates. *Eur. J. Inorg. Chem.* 2014, 2766–2772. doi: 10.1002/ejic.201301596
- Allain, C., Schaming, D., Karakostas, N., Erard, M., Gisselbrecht, J. P., Sorgues, S., et al. (2013). Synthesis, electrochemical and photophysical properties of covalently linked porphyrin-polyoxometalates. *Dalt. Trans.* 42, 2745–2754. doi: 10.1039/c2dt31415k
- Allen, C. C., Burns, R. C., Lawrance, G. A., Turner, P., and Hambley, T. W. (1997). Tetraammonium hexahydrogen-hexamolybdozincate(II) hexahydrate. *Acta Crystallogr. Sect. C Cryst. Struct. Commun.* 53(pt 1), 7–9. doi: 10.1107/S0108270196011043
- An, H., Li, Y., Xiao, D., Wang, E., and Sun, C. (2006). Self-assembly of extended high-dimensional architectures from Anderson-type polyoxometalate clusters. *Cryst. Growth Des.* 6, 1107–1112. doi: 10.1021/cg050326p
- An, H., Wang, E., Xiao, D., Li, Y., and Xu, L. (2005). Self-assembly of a novel 3D open framework from Anderson-type polyoxoanions. *Inorg. Chem. Commun.* 8, 267–270. doi: 10.1016/j.inoche.2004.12.024
- Anderson, J. S. (1937). Constitution of the polyacids. *Nature*. 140:850. doi: 10.1038/140850a0
- Aota, S., Nomizu, M., and Yamada, K. M. (1994). The short amino acid sequence Pro-His-Ser-Arg-Asn in human fibronectin enhances cell-adhesive function. *J. Biol. Chem.* 269, 24756–24761.
- Armelaio, L., Quici, S., Barigelletti, F., Accorsi, G., Bottaro, G., Cavazzini, M., et al. (2010). Design of luminescent lanthanide complexes: From molecules to highly efficient photo-emitting materials. *Coord. Chem. Rev.* 254, 487–505. doi: 10.1016/j.ccr.2009.07.025
- Bayraq, S. S., Nikseresht, A., and Khosravi, I. (2013). $(\text{NH}_4)_6\text{Mo}_7\text{O}_{34}\cdot 4\text{H}_2\text{O}$ as an efficient, selective, and reusable catalyst for the oxidation of thiols to disulfides using potassium bromate. *Phosphorus Sulfur Silicon Relat. Elem.* 188, 1236–1243. doi: 10.1080/10426507.2012.745076
- Bijelic, A., Molitor, C., Mauracher, S. G., Al-Oweini, R., Kortz, U., and Rompel, A. (2014). Hen egg-white lysozyme crystallisation: protein stacking and structure stability enhanced by a tellurium(VI)-centred polyoxotungstate. *ChemBioChem* 16, 233–241. doi: 10.1002/cbic.201402597
- Bijelic, A., and Rompel, A. (2015). The use of polyoxometalates in protein crystallography—an attempt to widen a well-known bottleneck. *Coord. Chem. Rev.* 299, 22–38. doi: 10.1016/j.ccr.2015.03.018
- Binnemans, K. (2009). Lanthanide-based luminescent hybrid materials. *Chem. Rev.* 109, 4283–4374. doi: 10.1021/cr8003983
- Blazevic, A., and Rompel, A. (2016). The Anderson-Evans polyoxometalate: from inorganic building blocks via hybrid organic-inorganic structures to tomorrow's 'Bio-POM'. *Coord. Chem. Rev.* 307, 42–64. doi: 10.1016/j.ccr.2015.07.001
- Bridgeman, A. J. (2006). Computational study of solvent effects and the vibrational spectra of the Anderson Polyoxometalates. *Chem. Eur. J.* 12, 2094–2102. doi: 10.1002/chem.200500802
- Bünzli, J. C. G., and Eliseeva, S. V. (2013). Intriguing aspects of lanthanide luminescence. *Chem. Sci.* 4, 1939–1949. doi: 10.1039/c3sc22126a
- Cao, R., Liu, S., Xie, L., Pan, Y., Cao, J., and Liu, Y. (2008). Influence of different site symmetries of Eu^{3+} centers on the luminescence properties of Anderson-based compounds. *Inorg. Chim. Acta* 361, 2013–2018. doi: 10.1016/j.ica.2007.10.015
- Charushnikova, I. A., Fedoseev, A. M., Yusov, A. B., and Den, A. C. (2005). Crystal structure of a new neodymium hexamolybdotellurate, $\text{Nd}_2\text{TeMo}_6\text{O}_{24}\cdot 19\text{H}_2\text{O}$. *Crystallogr. Reports* 50, 191–193. doi: 10.1134/1.1887892
- Coué, V., Dessapt, R., Bujoli-Doeuff, M., Evain, M., and Jobic, S. (2007). Synthesis, characterization, and photochromic properties of hybrid organic-inorganic materials based on molybdate, DABCO, and piperazine. *Inorg. Chem.* 46, 2824–2835. doi: 10.1021/ic0621502
- de Bettencourt-Dias, A. (ed.). (2014). *Luminescence of Lanthanide Ions in Coordination Compounds and Nanomaterials*. John Wiley and Sons, Ltd. doi: 10.1002/9781118682760
- Desiraju, G. R. (2007). Crystal engineering: a holistic view. *Angew. Chemie. Int. Ed.* 46, 8342–8356. doi: 10.1002/anie.200700534
- Desiraju, G. R., Vittal, J. J., and Ramanan, A. (2011). *Crystal Engineering: A Textbook*. World Scientific Publishing Co. Pvt. Ltd.
- Dhara, S., Dey, S., Basu, S., Drew, M. G. B., and Chattopadhyay, P. (2007). Separation of Ba-137m from Cs-137 using new ion exchanger $[\text{Na}_2(\text{H}_2\text{O})_4]_3[\text{Al}(\text{OH})_6\text{Mo}_6\text{O}_{18}]$. *Radiochim. Acta* 95, 297–301. doi: 10.1524/ract.2007.95.5.297
- Drewes, D., and Krebs, B. (2005). Synthesis and structure of a novel type of polyoxomolybdate lanthanide complex: $[(\text{Ln}(\text{H}_2\text{O})_6)_2(\text{TeMo}_6\text{O}_{24})]$ (Ln = Ho, Yb). *Zeitschrift für Anorg. und Allg. Chemie* 631, 2591–2594. doi: 10.1002/zaac.200500089
- Drewes, D., Limanski, E. M., and Krebs, B. (2004a). A series of novel lanthanide polyoxometalates: Condensation of building blocks dependent on the nature of rare earth cations. *Dalt. Trans.* 0, 2087–2091. doi: 10.1039/b404237a
- Drewes, D., Limanski, E. M., and Krebs, B. (2004b). The Anderson-type anion $(\text{TeMo}_6\text{O}_{24})^{6-}$ —a multidentate ligand for trivalent rare earth cations. *Eur. J. Inorg. Chem.* 2, 4849–4853. doi: 10.1002/ejic.200400525
- Eldik, R., and Cronin, L. (Eds.) (2017). *Advances in Inorganic Chemistry: Polyoxometalate Chemistry*, Vol. 69. Academic Press; Springer.
- Evans, H. T. (1948). The crystal structures of ammonium and potassium molybdotellurates. *J. Am. Chem. Soc.* 70, 1291–1292. doi: 10.1021/ja01183a521
- Fedoseev, A. M., Budantseva, N. A., Andreev, G. B., Yusov, A. B., and Shirokova, I. B. (2002). Hexamolybdoaluminates and hexamolybdochromates of some trivalent lanthanides and americium. *Russ. J. Coord. Chem. Khimiya* 28, 279–284. doi: 10.1023/A:1015276121718
- Feng, X., Zhou, W., Li, Y., Ke, H., Tang, J., Clérac, R., et al. (2012). Polyoxometalate-supported 3d-4f heterometallic single-molecule magnets. *Inorg. Chem.* 51, 2722–2724. doi: 10.1021/ic202418y
- Gao, B., Liu, S. X., Zhang, C. D., Xie, L. H., Sun, C. Y., and Yu, M. (2007). Hydrothermal assembly of pyrite-related framework: $(\text{NH}_4)_2\{[\text{Ni}(\text{H}_2\text{O})_3]_2[\text{TeW}_6\text{O}_{24}]\}\cdot \text{H}_2\text{O}$. *J. Coord. Chem.* 60, 911–918. doi: 10.1080/00958970600986075
- Gavrilova, L. O., and Molchanov, V. N. (2005). Heteropoly Complexes $\text{Na}_{0.5}\text{Cs}_{2-x}[\text{H}_{0.5-x}\text{M}_x^{\text{II}}\text{X}^{\text{III}}(\text{OH})_6\text{Mo}_6\text{O}_{18}] \cdot 7-8\text{H}_2\text{O}$ ($\text{M}^{\text{II}} = \text{Fe, Mn}$; $\text{X}^{\text{III}} = \text{Cr, Al}$). *Russ. J. Coord. Chem.* 31, 627–640. doi: 10.1007/s11173-005-0147-6

- Hakouk, K., Oms, O., Dolbecq, A., Marrot, J., Saad, A., Mialane, P., et al. (2014). New photoresponsive charge-transfer spiropyran/polyoxometalate assemblies with highly tunable optical properties. *J. Mater. Chem. C* 2, 1628–1641. doi: 10.1039/c3tc31992j
- He, Z., Yan, Y., Li, B., Ai, H., Wang, H., Li, H., et al. (2012). Thermal-induced dynamic self-assembly of adenine-grafted polyoxometalate complexes. *Dalt. Trans.* 41, 10043–10051. doi: 10.1039/c2dt30421j
- Hill, C. L. (1998). Introduction: polyoxometalates/multicomponent molecular vehicles to probe fundamental issues and practical problems. *Chem. Rev.* 98, 1–2. doi: 10.1021/cr960395y
- Himeno, S., Murata, S., and Eda, K. (2009). A route to a Keggin-Type α -[X(III)O₄Mo₁₂O₃₅(OH)]⁴⁻ anion through an Anderson-type [X(III)(OH)₆Mo₆O₁₈]³⁻ anion: X = Ga. *Dalt. Trans.* 35, 6114. doi: 10.1039/b902794g
- Hutin, M., Yvon, C., Yan, J., Macdonell, A., Long, D. L., and Cronin, L. (2013). Programming the assembly of carboxylic acid-functionalised hybrid polyoxometalates. *CrystEngComm* 15, 4422–4430. doi: 10.1039/c3ce26816k
- Inouye, Y., Tokutake, Y., Yoshida, T., Seto, Y., Hujita, H., Dan, K., et al. (1993). *In vitro* antiviral activity of polyoxomolybdates. Mechanism of inhibitory effect of PM-104 on human immunodeficiency virus type 1. *An. Tiviral Res.* 20, 317–331. doi: 10.1016/0166-3542(93)90075-T
- Ito, F., Ozeki, T., Ichida, H., Miyamae, H., and Sasaki, Y. (1989). Structure of tetraammonium hexahydrogenhexamolybdocuprate(II) tetrahydrate. *Acta Crystallogr. Sect. C* 45, 946–947. doi: 10.1107/S0108270188014544
- Ito, T., Yashiro, H., and Yamase, T. (2006). Regular two-dimensional molecular array of photoluminescent anderson-type polyoxometalate constructed by langmuir-blodgett technique. *Langmuir* 22, 2806–2810. doi: 10.1021/la052972w
- Joo, H. C., Park, K. M., Lee, U., and Brown, I. D. (2015). Crystal structure of the Anderson-type hetero-polyoxometalate; K₂[H₇Cr(III)Mo₆O₂₄]·8H₂O: A redetermination revealing the position of the extra H atom in the polyanion. *Acta Crystallogr. Sect. E Struct. Reports Online* 71, 157–160. doi: 10.1107/S2056989015000390
- Kitaigorodskii, A. I. (1965). The principle of close packing and the condition of thermodynamic stability of organic crystals. *Acta Crystallogr.* 18, 585–590. doi: 10.1107/S0365110X65001391
- Kondo, H., Kobayashi, A., and Sasaki, Y. (1980). The hexamolybdo-periodate anion in its potassium salt. *Acta Crystallogr. Sect. B* 36, 661–664. doi: 10.1107/S0567740880004037
- Kumar, D., Ahmad, S., Prakash, G. V., Ramanujachary, K. V., and Ramanan, A. (2014a). Photoluminescent chromium molybdate cluster coordinated with rare earth cations: synthesis, structure, optical and magnetic properties. *CrystEngComm* 16, 7097–7105. doi: 10.1039/c4ce00865k
- Kumar, D., Kumar, V., Upreti, S., and Ramanan, A. (2014b). Crystallization of hybrid molybdates based on organic bases. *Zeitschr. Anorg. Allg. Chem.* 640, 1190–1194. doi: 10.1002/zaac.201300687
- Kushch, L. A., Emel'yanov, V. A., Golhen, S., Cador, O., Schaniel, D., Woike, T., et al. (2009). The photochromic paramagnet derived from polyoxometalate [Cr(OH)₆Mo₆O₁₈]³⁻ and ruthenium mononitrosyl complex [RuNO(en)₂Cl]²⁺. *Inorg. Chim. Acta* 362, 2279–2282. doi: 10.1016/j.ica.2008.10.007
- Lee, H. Y., Park, K. M., Lee, U., and Ichida, H. (1991). Structure of tripotassium hexahydrogenhexamolybdoaluminate(III) heptahydrate. *Acta Crystallogr. Sect. C Cryst. Struct. Commun.* 47, 1959–1961. doi: 10.1107/S0108270191002159
- Lee, U. (1994). Dipotassium hexahydrogen- α -hexamolybdoplatinate(IV) pentahydrate, K₂[H₆ α -PtMo₆O₂₄]·5H₂O. *Acta Crystallogr. Sect. C Cryst. Struct. Commun.* 50, 1657–1659. doi: 10.1107/S0108270194001484
- Lee, U. (2007). Dipotassium heptahydrogenhexamolybdochromate(III) octahydrate, the first heptaprotonated Anderson-type polyoxometalate. *Acta Crystallogr. Sect. E Struct. Reports Online* 63, 7–9. doi: 10.1107/S1600536806052883
- Lee, U., and Joo, H. (2006a). Monopotassium monosodium hexahydrogen α -hexamolybdoplatinate(IV) hexahydrate. *Acta Cryst.* (2006). E62, i231–i233. doi: 10.1107/S1600536806043157
- Lee, U., and Joo, H. (2007). Hemiheptapotassium hemionahydrogen α -hexamolybdoplatinate(IV) 5.5-hydrate. *Acta Cryst.* (2007). E63, i11–i13. doi: 10.1107/S1600536806054055
- Lee, U., and Joo, H.-C. (2004). La₂[H₂PtMo₆O₂₄]·16H₂O. *Acta Cryst. E60*, i61–i63. doi: 10.1107/S1600536804007445
- Lee, U., Joo, H.-C., and Kwon, J.-S. (2002). Tetraammonium hexahydrogen hexamolybdonickelate(II) tetrahydrate, (NH₄)₄[H₆NiMo₆O₂₄]·4H₂O. *Acta Crystallogr. Sect. E Struct. Rep.* 58, i6–i8. doi: 10.1107/S1600536801021109
- Lee, U., Joo, H.-C., Kwon, J.-S., and Cho, M.-A. (2001). Tripotassium hexahydrogen hexamolybdocobaltate(III) heptahydrate, K₃[H₆CoMo₆O₂₄]·7H₂O. *Acta Crystallogr. Sect. E Struct. Rep.* 57, i112–i114. doi: 10.1107/S1600536801019365
- Lee, U., and Joo, H. C. (2000a). Tripotassium hexahydrogenhexamolybdocobaltate (III) potassium nitrate tetrahydrate, K₃[H₆CoMo₆O₂₄]·KNO₃·4H₂O. *Acta Crystallogr. Sect. C* 6–8. doi: 10.1107/S0108270100012154
- Lee, U., and Joo, H. C. (2000b). Dineodymium dihydrogen α -hexamolybdoplatinate(IV) tetradecahydrate, Nd₂[(H₂O)₂PtMo₆O₂₄]·14H₂O. *Acta Cryst.* c56, e311–e312. doi: 10.1107/S0108270100009689
- Lee, U., and Joo, H. C. (2006b). Dipotassium hexahydrogen hexamolybdo-platinate(IV) hexahydrate. *Acta Crystallogr. Sect. E Struct. Rep.* 62, 241–243. doi: 10.1107/S1600536806046125
- Lee, U., and Sasaki, Y. (1984). Isomerism of the hexamolybdo-platinate(IV) polyanion. Crystal structures of K_{3.5}[α -H_{4.5}PtMo₆O₂₄]·3H₂O and (NH₄)₄[β -H₄PtMo₆O₂₄]·1.5H₂O. *Chem. Lett.* 13, 1297–1300. doi: 10.1246/cl.1984.1297
- Lehmann, J., Gaita-Arino, A., Coronado, E., and Loss, D. (2007). Spin qubits with electrically gated polyoxometalate molecules. *Nat. Nanotechnol.* 2, 312–317. doi: 10.1038/nnano.2007.110
- Leuenberger, M. N., and Loss, D. (2001). Quantum computing in molecular magnets. *Nature* 410, 789–793. doi: 10.1038/35071024
- Li, B., Ye, L., and Wu, L.-X. (2011). [Al(H₂O)₆][Cr(OH)₆Mo₆O₁₈]·10H₂O. *Acta Crystallogr. Sect. E Struct. Rep.* 67, i8–i8. doi: 10.1107/S1600536810053936
- Li, F., and Xu, L. (2011). Coordination assemblies of polyoxomolybdate cluster framework: from labile building blocks to stable functional materials. *Dalt. Trans.* 40, 4024. doi: 10.1039/c0dt00691b
- Li, X. M., Guo, Y., Shi, T., and Chen, Y. G. (2016). Crystal structures and photoluminescence of two inorganic-organic hybrids of anderson anions. *J. Clust. Sci.* 27, 1913–1922. doi: 10.1007/s10876-016-1072-1
- Liu, B., Feng, L., Zhou, S., Li, C. B., and Zhou, W. (2007). Poly[diammonium diaqua-hexahydroxyoctadeca-oxodisodiohexamolybdonickelate(II)]. *Acta Crystallogr. Sect. E Struct. Rep.* 63, 14–15. doi: 10.1107/S1600536806053761
- Liu, B., Zhou, S., Li, C. B., and Zhang, H. G. (2006). Poly[bis(imidazolium) hexahydroxyoctadeca-oxodisodiohexamolybdonickelate dihydrate]. *Acta Crystallogr. Sect. E Struct. Rep.* 62, 3188–3190. doi: 10.1107/S1600536806045168
- Liu, F.-X., Marchal-Roch, C., Dambournet, D., Acker, A., Marrot, J., and Sécheresse, F. (2008). From molecular to two-dimensional anderson polyoxomolybdate: synthesis, crystal structure, and thermal behavior of [(Ni(H₂O)₄]₂[Ni(OH)₆Mo₆O₁₈]]·4H₂O and [Ni(H₂O)₆][Ag₂[Ni(OH)₆Mo₆O₁₈]]·8H₂O. *Eur. J. Inorg. Chem.* 2008, 2191–2198. doi: 10.1002/ejic.200701288
- Liu, Y., Liu, S. X., Cao, R. G., Ji, H. M., Zhang, S. W., and Ren, Y. H. (2008). Hydrothermal assembly and luminescence property of lanthanide-containing Anderson polyoxometalates. *J. Solid State Chem.* 181, 2237–2242. doi: 10.1016/j.jssc.2008.05.023
- Lorenzo-Luis, P. A., Gili, P., Sánchez, A., Rodríguez-Castellón, E., Jiménez-Jiménez, J., Ruiz-Pérez, C., et al. (1999). Tungstotellurates of the imidazolium and 4-methylimidazolium cations. *Transit. Met. Chem.* 24, 686–692. doi: 10.1023/A1006987412453
- Lundberg, D., Persson, I., Eriksson, L., D'Angelo, P., and Panfilis, S. De. (2010). Structural study of the N,N'-dimethylpropyleneurea solvated lanthanoid(III) ions in solution and solid state with an analysis of the ionic radii of lanthanoid(III) ions. *Inorg. Chem.* 49, 4420–4432. doi: 10.1021/ic100034q
- Manikumari, S., Shivaiah, V., and Das, S. K. (2002). Identification of a near-linear supramolecular water dimer, (H₂O)₂, in the channel of an inorganic framework material. *Inorg. Chem.* 41, 6953–6955. doi: 10.1021/ic025803x
- Martin, C., Lamonier, C., Fournier, M., Mentré, O., Harlé, V., Guillaume, D., et al. (2004). Preparation and characterization of 6-molybdocobaltate and 6-molybdoaluminate cobalt salts. Evidence of a new heteropolymolybdate structure. *Inorg. Chem.* 43, 4636–4644. doi: 10.1021/ic0354365
- Massia, S. P., and Hubbell, J. A. (1991). An RGD spacing of 440 nm is sufficient for integrin α -V- β -3-mediated fibroblast spreading and 140 nm for

- focal contact and stress fiber formation. *J. Cell Biol.* 114, 1089–1100. doi: 10.1083/jcb.114.5.1089
- Mauracher, S. G., Molitor, C., Al-Oweini, R., Kortz, U., and Rompel, A. (2014a). Latent and active abPPO4 mushroom tyrosinase cocrystallized with hexatungstotellurate(VI) in a single crystal. *Acta Crystallogr. Sect. D Biol. Crystallogr.* 70, 2301–2315. doi: 10.1107/S1399004714013777
- Mauracher, S. G., Molitor, C., Al-Oweini, R., Kortz, U., and Rompel, A. (2014b). Crystallization and preliminary X-ray crystallographic analysis of latent isoform PPO4 mushroom (*Agaricus bisporus*) tyrosinase. *Acta Crystallogr. Sect. F Struct. Biol. Commun.* 70, 263–266. doi: 10.1107/S2053230X14000582
- Mensinger, Z. L., Zakharov, L. N., and Johnson, D. W. (2008). Triammonium hexahydroxidooctadeca-oxidohexamolybdogallate(III) hepta-hydrate. *Acta Crystallogr. Sect. E Struct. Rep.* 64, i8–i9. doi: 10.1107/S1600536807068067
- Michailovski, A., Hussain, F., and Spingler, B. (2009). Hydrothermal strategies towards polyoxofluoromolybdates (VI). *Cryst. Growth Des.* 9, 755–765. doi: 10.1021/cg800265q
- Nolan, A. L., Burns, R. C., and Lawrance, G. A. (1996). Reaction kinetics and mechanism of formation of $[H_4Co_2Mo_{10}O_{38}]^{6-}$ by peroxomonosulphate oxidation of Co(II) in the presence of molybdate. *J. Chem. Soc. Dalton Trans.* 20, 2629–2636. doi: 10.1039/DT9850002629
- Ogawa, A., Yamato, H., Lee, U., Ichida, H., Kobayashi, A., and Sasaki, Y. (1988). Structure of pentapotassium dihydrogenhexamolybdoantimonate heptahydrate. *Acta Crystallogr. Sect. C Cryst. Struct. Commun.* 44, 1879–1881. doi: 10.1107/S0108270188007073
- Ohashi, K., Yanagi, K., Sasada, Y., and Yamase, T. (1982). Crystal Structure and Photochemistry of Isopolymolybdates. I. The crystal structures of hexaki(propylammonium)heptamolybdate(VI) trihydrate and hexakis(isopropylammonium)heptamolybdate(VI) trihydrate. *Bull. Chem. Soc. Jpn.* 55, 1254–1260. doi: 10.1246/bcsj.55.1254
- Oms, O., Hakouk, K., Dessapt, R., Deniard, P., Jobic, S., Dolbecq, A., et al. (2012). Photo- and electrochromic properties of covalently connected symmetrical and unsymmetrical spiropyran-polyoxometalate dyads. *Chem. Commun.* 48, 12103–12105. doi: 10.1039/c2cc35376h
- Ozawa, Y., Hayashi, Y., and Isobe, K. (1991). Structure of triammonium hexahydrogenhexamolybdoorthodate(III) hexahydrate. *Acta Crystallogr. Sect. C* 47, 637–638. doi: 10.1107/S0108270190009763
- Panneerselvam, K., Soriano-García, M., Holguin-Quiñones, S., and Holt, E. M. (1996). Hexa-aqua-gallium hexahydrogenhexamolybdocobaltate(III) decahydrate. *Acta Crystallogr. Sect. C Cryst. Struct. Commun.* 52, 1605–1607. doi: 10.1107/S0108270195017161
- Pardo, R., Zayat, M., and Levy, D. (2011). Photochromic organic-inorganic hybrid materials. *Chem. Soc. Rev.* 40, 672–687. doi: 10.1039/c0cs00065e
- Pavani, K., Singh, M., and Ramanan, A. (2011). Oxalate bridged copper pyrazole complex templated Anderson-Evans cluster based solids. *Aust. J. Chem.* 64, 68–76. doi: 10.1071/CH10276
- Perloff, A. (1970). The crystal structure of sodium hexamolybdochromate(III) Octahydrate, $Na_3(CrMo_6O_{24}H_6) \cdot 8H_2O$. *Inorg. Chem.* 9, 2228–2239. doi: 10.1021/ic50092a006
- Pope, M. T. (1983). *Heteropoly and Isopoly Oxometalates*. Berlin; Heidelberg: Springer-Verlag.
- Pope, M. T. (2002). *Polyoxometalate Chemistry From Topology via Self-Assembly to Applications*. Kluwer Academic Publishers.
- Pradeesh, K., Baumberg, J. J., and Prakash, G. V. (2009). Strong exciton-photon coupling in inorganic-organic multiple quantum wells embedded low-Q microcavity. *Opt. Express* 17:22171. doi: 10.1364/OE.17.022171
- Raza, R., Matin, A., Sarwar, S., Barsukova-Stuckart, M., Ibrahim, M., Kortz, U., et al. (2012). Polyoxometalates as potent and selective inhibitors of alkaline phosphatases with profound anticancer and amoebicidal activities. *Dalt. Trans.* 41, 14329–14336. doi: 10.1039/c2dt31784b
- Ritchie, C., and Bryant, G. (2015). Microwave assisted synthesis of a mono organoimido functionalized Anderson polyoxometalate. *Dalt. Trans.* 44, 20826–20829. doi: 10.1039/c5dt04000k
- Robl, C., and Frost, M. (1993a). $Na_6[TeMo_6O_{24}] \cdot 22H_2O$ —a layered heteropoly compound with the chain-like polycation $[Na_3(H_2O)_{11}]_n^{3n+}$. *Z. Naturforsch.* 48b, 404–408. doi: 10.1515/znb-1993-0402
- Robl, C., and Frost, M. (1993b). Alkalimolybdo-tellurate: Darstellung und Kristallstruktur von $Rb_6[TeMo_6O_{24}] \cdot 10H_2O$ und $Rb_6[TeMo_6O_{24}] \cdot Te(OH)_6 \cdot 6H_2O$. *Z. Anorg. Allg. Chem.* 619, 1834–1840. doi: 10.1002/zaac.19936191105
- Rosnes, M. Ali, H., Yvon, C., Long, D. L., and Cronin, L. (2012). Mapping the synthesis of low nuclearity polyoxometalates from octamolybdates to Mn-Anderson cluster. *Dalt. Trans.* 41, 10071–10079. doi: 10.1039/c2dt31008b
- Rosnes, M. H., Musumeci, C., Yvon, C., Macdonell, A., Pradeep, C. P., Sartorio, C., et al. (2013). Exploring the interplay between ligand derivatisation and cation type in the assembly of hybrid polyoxometalate Mn-andersons. *Small* 9, 2316–2324. doi: 10.1002/sml.201202510
- Rosu, C., and Weakley, T. J. R. (2000). Disodium chromium(III) hexamolybdoiodate(VII) 24-hydrate, $Na_2Cr[IMo_6O_{24}] \cdot 24H_2O$. *Acta Crystallogr. Sect. C*, C56, e170–e171.
- Schaming, D., Allain, C., Farha, R., Goldmann, M., Lobstein, S., Giraudeau, A., et al. (2010). Synthesis and photocatalytic properties of mixed polyoxometalate-porphyrin copolymers obtained from anderson-type polyoxomolybdates. *Langmuir* 26, 5101–5109. doi: 10.1021/la903564d
- Shah, H. S., Al-Oweini, R., Haider, A., Kortz, U., and Iqbal, J. (2014). Cytotoxicity and enzyme inhibition studies of polyoxometalates and their chitosan nanoassemblies. *Toxicol. Rep.* 1, 341–352. doi: 10.1016/j.toxrep.2014.06.001
- Shannon, R. D. (1976). Revised effective ionic radii and systematic studies of interatomic distances in halides and chalcogenides. *Acta Crystallogr.* A32, 751–767. doi: 10.1107/S0567739476001551
- Shi, D., Hu, M., Zhang, C., Li, J., and Chen, Y. (2008). Synthesis and structure of a novel polyoxomolybdate lanthanide complex: $[Er_2(H_2O)_{14}Cr(OH)_6Mo_6O_{18}][Cr(OH)_6Mo_6O_{18}] \cdot 14H_2O$. *J. Chem. Crystallogr.* 38, 695–700. doi: 10.1007/s10870-008-9378-y
- Shi, D. M., Ma, F. X., Zhang, C. J., Lu, S., and Chen, Y. G. (2008). Self-assembly of polyoxometalate-supported Ln-H hydroxo/oxo clusters with 1D extended structure: $[LnIII(H_2O)_7Cr(OH)_6Mo_6O_{18}]_n \cdot 4nH_2O$ (Ln = Ce, Sm, Eu). *Zeitschr. Anorg. und Allg. Chemie* 634, 758–763. doi: 10.1002/zaac.200700498
- Shivaiah, V., Chatterjee, T., and Das, S. K. (2014). Coordination of lanthanide cation to an Anderson type polyoxometalate anion leads to isomorphous metal-oxide based one-dimensional inorganic solids: synthesis, crystal structure and spectroscopy. *J. Chem. Sci.* 126, 1525–1533. doi: 10.1007/s12039-014-0688-7
- Shivaiah, V., and Das, S. K. (2005). Supramolecular assembly based on a heteropolyanion: synthesis and crystal structure of $Na_3(H_2O)_6[Al(OH)_6Mo_6O_{18}] \cdot 2H_2O$. *J. Chem. Sci.* 117, 227–233. doi: 10.1007/BF02709291
- Shivaiah, V., Nagaraju, M., and Das, S. K. (2003). Formation of a spiral-shaped inorganic-organic hybrid chain, $[Cu(II)(2,2'-bipy)(H_2O)2Al(OH)_6Mo_6O_{18}]$: Influence of intra- and interchain supramolecular interactions. *Inorg. Chem.* 42, 6604–6606. doi: 10.1021/ic034581f
- Shivaiah, V., Narasimha Reddy, P. V., Cronin, L., and Das, S. K. (2002). A novel polyoxometalate chain formed from heteropolyanion building blocks and rare earth metal ion linkers: $[La(H_2O)_7Al(OH)_6Mo_6O_{18}]_n \cdot 4nH_2O$. *J. Chem. Soc. Dalton Trans.* 1, 3781–3782. doi: 10.1039/B207149E
- Singh, M., Kumar, D., and Ramanan, A. (2014). Crystal engineering of Anderson-Evans cluster based salts through N-H...O interactions. *Proc. Natl. Acad. Sci. India Sect. A Phys. Sci.* 84, 305–314. doi: 10.1007/s40010-014-0144-6
- Singh, M., Kumar, D., Thomas, J., and Ramanan, A. (2010a). Crystallization of copper(II) sulfate based minerals and MOF from solution: chemical insights into the supramolecular interactions. *J. Chem. Sci.* 122, 757–769. doi: 10.1007/s12039-010-0064-1
- Singh, M., Lofland, S. E., Ramanujachary, K. V., and Ramanan, A. (2010b). Crystallization of Anderson-Evans type chromium molybdate solids incorporated with a metal pyrazine complex or coordination polymer. *Cryst. Growth Des.* 10, 5105–5112. doi: 10.1021/cg100754k
- Singh, M., and Ramanan, A. (2011). Crystal engineering of polyoxomolybdates based metal-organic solids: the case of chromium molybdate cluster based metal complexes and coordination polymers. *Cryst. Growth Des.* 11, 3381–3394. doi: 10.1021/cg101695w
- Song, P. Y.-F. (2018). *Polyoxometalate-Based Assemblies and Functional Materials*. Springer International Publishing.
- Song, Y. F., McMillan, N., Long, D. L., Kane, S., Malm, J., Riehle, M. O., et al. (2009). Micropatterned surfaces with covalently grafted unsymmetrical polyoxometalate-hybrid clusters lead to selective cell adhesion. *J. Am. Chem. Soc.* 131, 1340–1341. doi: 10.1021/ja807091v

- Song, Y. F., McMillan, N., Long, D. L., Thiel, J., Ding, Y., Chen, H., et al. (2008). Design of hydrophobic polyoxometalate hybrid assemblies beyond surfactant encapsulation. *Chem. A Eur. J.* 14, 2349–2354. doi: 10.1002/chem.200701629
- Swapna, K., Mahamuda, S., Rao, A. S., Sasikala, T., Packiyaraj, P., Moorthy, L. R., et al. (2014). Luminescence characterization of Eu³⁺ doped zinc alumino bismuth borate glasses for visible red emission applications. *J. Lumin.* 156, 80–86. doi: 10.1016/j.jlumin.2014.07.022
- Tanaka, S., Annaka, M., and Sakai, K. (2012). Visible light-induced water oxidation catalyzed by molybdenum-based polyoxometalates with mono- and dicobalt(III) cores as oxygen-evolving centers. *Chem. Commun.* 48, 1653–1655. doi: 10.1039/c2cc16821a
- Tkac, P., and Paulenova, A. (2008). Speciation of molybdenum (VI) in aqueous and organic phases of selected extraction systems. *Sep. Sci. Technol.* 43, 2641–2657. doi: 10.1080/01496390802122261
- Upreti, S., Datta, A., and Ramanan, A. (2007). Role of nonbonding interactions in the crystal growth of phenazinediamine tetrahydrate: new insights into the occurrence of 2D water layers in crystal hydrates. *Cryst. Growth Des.* 7, 966–971. doi: 10.1021/cg060958r
- Wang, H. Y., Zhang, C. J., Zhang, C. H., Tang, Q., and Chen, Y. G. (2011). Synthesis, structure, and magnetism of four polyoxomolybdate compounds containing yttrium and ytterbium. *J. Coord. Chem.* 64, 1481–1490. doi: 10.1080/00958972.2011.573847
- Weber, M. J. (1973). Chromium—rare-earth energy transfer in YAlO₃. *J. Appl. Phys.* 44, 4058–4064. doi: 10.1063/1.1662895
- Wu, C., Lin, X., Yu, R., Yang, W., Lu, C., and Zhuang, H. (2001). [Na₄(H₂O)₇][Fe(OH)₆Mo₆O₁₈]: A new [12] metallocrown-6 structure with an octahedrally coordinated iron at the center. *Sci. China Ser. B Chem.* 44, 49–54. doi: 10.1007/BF02879735
- Wu, Q., Li, Y. G., Wang, Y. H., Clérac, R., Lu, Y., and Wang, E. B. (2009). Polyoxometalate-based {Mn^{III}₂}-Schiff base composite materials exhibiting single-molecule magnet behaviour. *Chem. Commun.* 38, 5743–5745. doi: 10.1039/b909246c
- Yamase, T. (1993). Polyoxometalates for molecular devices: antitumor activity and luminescence. *Mol. Eng.* 3, 241–262. doi: 10.1007/BF00999636
- Yamase, T., and Sugeta, M. (1993). Charge-transfer photoluminescence of polyoxo-tungstates and -molybdates. *J. Chem. Soc. Dalton Trans.* 0, 759–765. doi: 10.1039/DT9930000759
- Yan, J., Gong, K., Xue, X., He, X., Zhao, C., Han, Z., et al. (2014). Two layerlike supramolecular assemblies based on B-Anderson-type polyanionic clusters and their adsorption property. *Eur. J. Inorg. Chem.* 2014, 5969–5976. doi: 10.1002/ejic.201402654
- Yan, X., Mo, S., Ju, Z., Wu, J., and Yao, K. (2008). Synthesis and structure of a series of Anderson-Evans type heteropolymolybdates: [Ln(H₂O)_n]₂[TeMo₆O₂₄]·6H₂O. *Synth. React. Inorg. Met. Nano-Metal Chem.* 38, 529–533. doi: 10.1080/15533170802265459
- Yan, Y., Li, B., He, Q., He, Z., Ai, H., Wang, H., et al. (2012). Synthesis and redox-responsive self-assembly of ferrocene grafted Anderson-type polyoxometalate hybrid complexes. *Soft Matter* 8, 1593–1600. doi: 10.1039/c1sm06610b
- Yang, L., Zhou, Z., Ma, P.-T., Zhang, X.-F., Wang, J.-P., and Niu, J.-Y. (2013). Three organic-inorganic hybrid B-Anderson polyoxoanions as building blocks: syntheses, structures, and characterization of [(C₆H₅NO₂)₂Ln(H₂O)₆](CrMo₆O₂₄H₆)·2C₆H₅NO₂·6H₂O (Ln = Sm, Dy, Er). *J. Coord. Chem.* 66, 1058–1067. doi: 10.1080/00958972.2013.775429
- Yu, L., Li, S.-Z., and Wang, J.-P. (2006). [Na₃(H₂O)₁₁][CrMo₆O₂₄H₆]·2H₂O, with an Anderson B-type heteropolyoxoanion. *Acta Crystallogr. Sect. E Struct. Rep.* 62, i190–i192. doi: 10.1107/S1600536806032910
- Yusov, A. B., Yin, M., Fedosseev, A. M., Andreev, G. B., Shirokova, I. B., and Krupa, J.-C. (2002). Luminescence study of new Ln(III) compounds formed from Anderson's heteropoly anions {Al(OH)₆Mo₆O₁₈}³⁻ and {Cr(OH)₆Mo₆O₁₈}³⁻. *J. Alloys Compd.* 344, 289–292. doi: 10.1016/S0925-8388(02)0371-7
- Yvon, C., Surman, A. J., Hutin, M., Alex, J., Smith, B. O., Long, D. L., et al. (2014). Polyoxometalate clusters integrated into peptide chains and as inorganic amino acids: Solution- and solid-phase approaches. *Angew. Chem. Int. Ed.* 53, 3336–3341. doi: 10.1002/anie.201311135
- Zhang, J., Huang, Y., Hao, J., and Wei, Y. (2017). β-[Cr[RC(CH₂O)₃]₂Mo₆O₁₈]³⁻: The first organically-functionalized β isomer of Anderson-type polyoxometalates. *Inorg. Chem. Front.* 4, 1215–1218. doi: 10.1039/c7qi00199a
- Zhang, J., Liu, Z., Huang, Y., Zhang, J., Hao, J., and Wei, Y. (2015a). Unprecedented χ isomers of single-side triol-functionalized Anderson polyoxometalates and their proton-controlled isomer transformation. *Chem. Commun.* 51, 9097–9100. doi: 10.1039/c5cc02947c
- Zhang, J., Luo, J., Wang, P., Ding, B., Huang, Y., Zhao, Z., et al. (2015b). Step-by-step strategy from achiral precursors to polyoxometalates-based chiral organic-inorganic hybrids. *Inorg. Chem.* 54, 2551–2559. doi: 10.1021/ic502622k
- Zhang, J., Yin, P., Hao, J., Xiao, F., Chen, L., and Wei, Y. (2012). Synthesis and assembly of a difunctional core POM cluster with two appended POM cluster caps. *Chem. A Eur. J.* 18, 13596–13599. doi: 10.1002/chem.201201098
- Zhang, J., Zhao, Z., Zhang, J., She, S., Huang, Y., and Wei, Y. (2014). Spontaneous resolution of polyoxometalate-based inorganic-organic hybrids driven by solvent and common ion. *Dalt. Trans.* 43, 17296–17302. doi: 10.1039/c4dt01954g
- Zhang, L. Z., Gu, W., Dong, Z. L., Liu, X., and Li, B. (2008). Phase transformation of a rare-earth Anderson polyoxometalate at low temperature. *Crystengcomm* 10, 1318–1320. doi: 10.1039/b808085b
- Zhao, L., Shen, S., and Yu, H. (2008). Synthesis, crystal structure and characterization of a 1D polyoxometalate-based compound: {[Pr(H₂O)₇][CrMo₆H₆O₂₄]·4H₂O}. *Z. Naturforsch.* 63b, 799–803. doi: 10.1515/znb-2008-0702
- Zhou, D. P., and Yang, D. (2007). A new chain-like polyoxometallate based on B-Anderson-type building blocks and rare earth metal ion linkers. *Acta Crystallogr. Sect. E Struct. Rep.* 63, 113–115. doi: 10.1107/S1600536807007787
- Zhou, Y. H., Zhao, M., Sun, H., Mao, Z. W., and Ji, L. N. (2009). Effect of cyclodextrin dimers with bipyridyl and biphenyl linking groups on carboxyl ester hydrolysis catalyzed by zinc complex. *J. Mol. Catal. A Chem.* 308, 61–67. doi: 10.1016/j.molcata.2009.03.026

Conflict of Interest Statement: The authors declare that the research was conducted in the absence of any commercial or financial relationships that could be construed as a potential conflict of interest.

Copyright © 2019 Tewari, Adnan, Balendra, Kumar, Jangra, Prakash and Ramanan. This is an open-access article distributed under the terms of the Creative Commons Attribution License (CC BY). The use, distribution or reproduction in other forums is permitted, provided the original author(s) and the copyright owner(s) are credited and that the original publication in this journal is cited, in accordance with accepted academic practice. No use, distribution or reproduction is permitted which does not comply with these terms.